GENETICS

Decoupling the role of RORγt in the differentiation and effector function of T$_H$17 cells

Xiancai Zhong[1], Hongmin Wu[1], Wencan Zhang[1], Yousang Gwack[2], Weirong Shang[3], Kyle O. Lee[4], Noah Isakov[5], Zhiheng He[1]*†, Zuoming Sun[1]*

RORγt is known to instruct the differentiation of T helper 17 (T$_H$17) cells that mediate the pathogenesis of autoimmune diseases. However, it remains unknown whether RORγt plays a distinct role in the differentiation and effector function of T$_H$17 cells. Here, we show that mutation of RORγt lysine-256, a ubiquitination site, to arginine (K256R) separates the RORγt role in these two functions. Preventing ubiquitination at K256 via arginine substitution does not affect RORγt-dependent thymocyte development, and T$_H$17 differentiation in vitro and in vivo, however, greatly impaired the pathogenesis of T$_H$17 cell–mediated experimental autoimmune encephalomyelitis (EAE). Mechanistically, K256R mutation impairs RORγt to bind to and activate *Runx1* expression critical for T$_H$17-mediated EAE. Thus, RORγt regulates the effector function of T$_H$17 cells in addition to T$_H$17 differentiation. This work informs the development of RORγt-based therapies that specifically target the effector function of T$_H$17 cells responsible for autoimmunity.

INTRODUCTION

Interleukin-17 (IL-17)–producing CD4$^+$ T helper, or T helper 17, (T$_H$17) cells participate in immune responses against pathogens and the pathogenesis of diverse immunological diseases such as autoimmune diseases and even autism (*1–6*). The transcription factor retinoid-related orphan receptor γt (RORγt), encoded by the gene *Rorc*, instructs the differentiation of T$_H$17 cells (*7–9*). Mutations in *Rorc* affect IL-17 production and lead to severe immune deficiency in both mouse (*7*) and human (*10*). Thus, therapies that control the pathogenic T$_H$17 responses are needed clinically (*11, 12*). Numerous pharmacological RORγt inhibitors have been developed for clinical application (*5, 11–13*). Those inhibitors are believed to prevent T$_H$17-dependent autoimmunity by inhibiting the generation of T$_H$17 cells due to the essential function of RORγt in T$_H$17 differentiation.

The strength of the T$_H$17 immune responses is determined by the overall number of T$_H$17 cells and their effector function. T$_H$17 cells are derived from naïve CD4$^+$ T cells upon activation in the presence of an appropriate cytokine milieu including IL-6, transforming growth factor–β (TGF-β), and/or IL-23 (*7, 14*). Although the function of RORγt in T$_H$17 differentiation has long been demonstrated, it remains unknown whether RORγt plays a role in the effector function of T$_H$17 cells and whether RORγt has a distinct role in the differentiation versus effector function of T$_H$17 cells. In addition to regulating T$_H$17 cells, RORγt enhances thymocyte survival (*15–18*) and is required for lymph node development (*8, 18–20*). Previously, we have generated a mutation in RORγt that disrupts T$_H$17 differentiation but not thymocyte development (*8*), indicating that RORγt uses different mechanisms to regulate the function of T$_H$17 cells and thymocytes.

Ubiquitination is a posttranslational modification that regulates many aspects of cellular function (*21*). Ubiquitin is conjugated to the lysine residues of the proteins to modulate protein function by regulating protein stability and/or protein-protein interactions. Thus, cellular context-dependent ubiquitination of RORγt may be a mechanism to modulate the diverse RORγt functions. In vitro studies indicate the regulation of RORγt stability by ubiquitination (*22–25*). However, in vivo function of RORγt ubiquitination is difficult to prove, as it requires the generation of the mice expressing mutant RORγt incapable of being ubiquitinated. Previous studies used mice deficient in ubiquitin ligases or deubiquitinases to understand the role of ubiquitination in immune responses (*26*). Such an approach prevents the ubiquitination of all the substrates; thus, it is impossible to determine the function of a specific substrate and even less about the function of a specific ubiquitination site on the substrate in immunological function.

In this study, three in vitro assays were developed to dissect RORγt function in thymocyte development, T$_H$17 differentiation, and effector function in experimental autoimmune encephalomyelitis (EAE) induction. A RORγt mutation at a ubiquitination site, lysine (K)–256 to arginine (RORγt^{K256R}), was found to specifically impair the effector function of T$_H$17 cells in inducing EAE without interfering with RORγt function in T$_H$17 differentiation and thymocyte development. A strain of mice was established to express RORγt^{K256R} (*RORγt$^{K256R/K256R}$*), which cannot be ubiquitinated at this site. This strain of mice allows us to determine the in vivo function of ubiquitination of RORγt at a specific site. *RORγt$^{K256R/K256R}$* mice have normal thymocyte development, lymph node development, and T$_H$17 differentiation. However, *RORγt$^{K256R/K256R}$* mice display greatly impaired T$_H$17 immune responses leading to EAE. Further, *RORγt$^{K256R/K256R}$* T$_H$17 cells showed decreased RORγt^{K256R} binding to the promoter region of the *Runx1* gene and reduced expression of *Runx1*. Forced expression of *Runx1* in *RORγt$^{K256R/K256R}$* T$_H$17 cells restored the ability to induce EAE. Therefore, RORγt regulates the effector function of T$_H$17 cells in addition to T$_H$17 differentiation.

[1]Department of Immunology and Theranostics, Arthur Riggs Diabetes and Metabolism Research Institute, Beckman Research Institute of the City of Hope, Duarte, CA 91010, USA. [2]Department of Physiology, David Geffen School of Medicine, UCLA, Los Angeles, CA 90095, USA. [3]Department of Gynecology and Obstetrics, School of Medicine, Emory University, Atlanta, GA 30322, USA. [4]Eugene and Ruth Roberts Summer Student Academy, City of Hope, Duarte, CA 91010, USA. [5]Department of Microbiology, Immunology, and Genetics, Ben-Gurion University of the Negev, Beer Sheva, Israel.
*Corresponding author. Email: zhe@wakehealth.edu (Z.H.); zsun@coh.org (Z.S.)
†Present address: Department of Microbiology and Immunology, Wake Forest University School of Medicine, Winston-Salem, NC 277101, USA.

RESULTS

Three assays are developed to dissect RORγt function

$ROR\gamma t^{-/-}$ mice display defects in thymic T cell development, T_H17 differentiation, and development of T_H17-dependent EAE (7, 18). To dissect the function of RORγt, we developed three assays to separate these three functions. To determine the function of RORγt in thymocytes, we used an in vitro thymocyte differentiation system (27). $CD4^-CD8^-$ thymocytes from wild-type (WT) but not $ROR\gamma t^{-/-}$ mice could differentiate into $CD4^+CD8^+$ and $CD4^+$ cells (Fig. 1A). Consistently, $ROR\gamma t^{-/-}$ $CD4^-CD8^-$ thymocytes transduced with a retrovirus expressing a RORγt (RORγt) but not green fluorescent protein (GFP) alone [empty virus (EV)] rescued the development of $CD4^+CD8^+$ and $CD4^+$ from $ROR\gamma t^{-/-}$ thymocyte (Fig. 1B and fig. S1A for gating strategy). We next used an in vitro assay to determine the function of RORγt in T_H17 differentiation. Under T_H17 polarization conditions, $ROR\gamma t^{-/-}$ naïve $CD4^+$ T cells could not differentiate into T_H17 cells unless exogenous RORγt was provided via retrovirus transduction (Fig. 1C and fig. S1B for gating strategy). Last, adoptive transfer EAE model enabled the testing of RORγt T_H17 effector function by using 2D2 T cell receptor (TCR) transgenic mice (Tg^{Tcr2D2}) that recognize myelin oligodendrocyte glycoprotein (MOG_{35-55}) (28, 29). $ROR\gamma t^{-/-}/Tg^{Tcr2D2}$ $CD4^+$ T cells were transduced with virus expressing RORγt, polarized under T_H17 conditions and adoptively transferred into $Rag1^{-/-}$ recipients for inducing EAE (30). $ROR\gamma t^{-/-}/Tg^{Tcr2D2}$ $CD4^+$ T cells expressing RORγt induced very severe EAE ($ROR\gamma t^{-/-}/Tg^{Tcr2D2}$ + RORγt); these mice had the highest disease score of 5 (the Institutional Animal Care and Use Committee protocol does not permit disease development beyond

this point) equivalent to $Rag1^{-/-}$ recipients with WT Tg^{Tcr2D2} $CD4^+$ T cells transduced with GFP alone (WT Tg^{Tcr2D2} + EV) (Fig. 1D). In contrast, $ROR\gamma t^{-/-}/Tg^{Tcr2D2}$ $CD4^+$ T cells expressing GFP alone ($ROR\gamma t^{-/-}/Tg^{Tcr2D2}$ + EV) resulted in greatly delayed and impaired EAE with the highest disease score of 3. RORγt deficiency did not affect the proliferation and survival of Tg^{Tcr2D2} $CD4^+$ T cells in vitro (fig. S1, C and D) and in vivo (fig. S1E), which is also indicated by an equivalent number $CD4^+$ T cells recovered from the spleen after adoptive transfer (fig. S1F). The successful establishment of above assays allowed us to dissect three RORγt-regulated functions.

RORγt-K256, a ubiquitination site, is critical for the effector function but not the differentiation of T_H17 cells

RORγt has been shown to regulate T_H17 differentiation; it, however, remains unknown whether and how RORγt regulates the effector function of T_H17 cells. To address this question, we aimed to identify RORγt mutations that specifically disrupt RORγt function in effector T_H17 cell–mediated EAE but not in T_H17 differentiation and thymocyte development. Previously, we mutated lysine residues (K) on RORγt to arginine (R) to study the function of posttranslational modification of RORγt (8). Thus, we first compared the ability of WT and RORγt mutants to rescue $ROR\gamma t^{-/-}$ thymocyte development. Only RORγt-K31R mutation moderately affected thymocyte development (Fig. 2A). In terms of T_H17 differentiation, K31R, K69R, and K313R impaired T_H17 differentiation (Fig. 2, B to D), consistent with our published results (8, 9, 31). Further, most RORγt mutations either impaired or potentiated T_H17 differentiation (Fig. 2B),
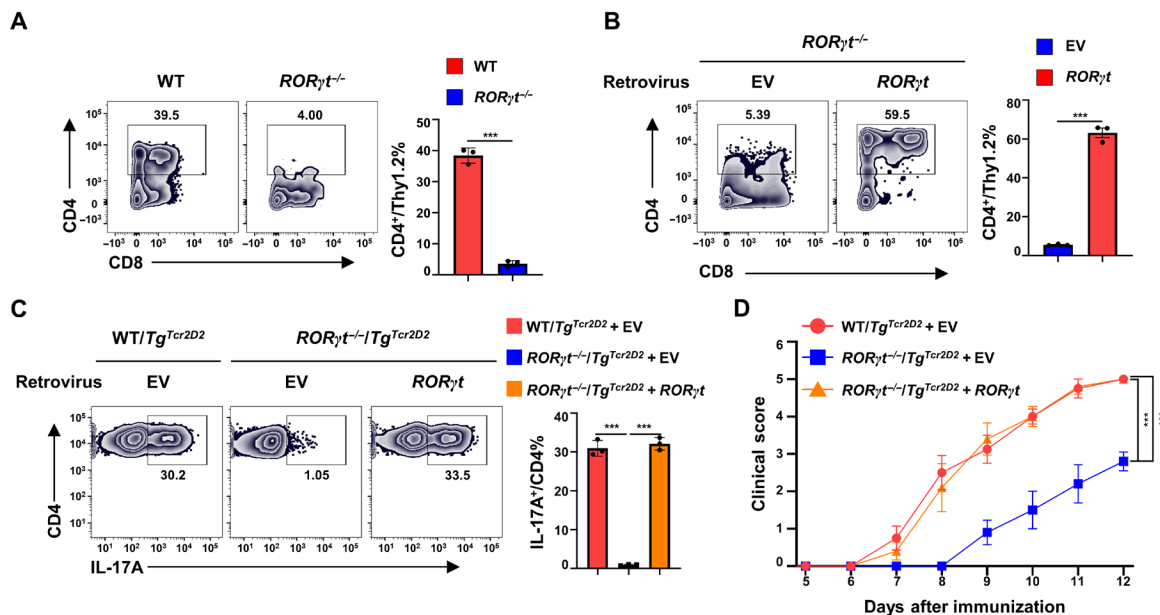
Fig. 1. Three assays are developed to dissect RORγt function. (**A**) Representative flow cytometric analysis (left) of $CD4^+$ and $CD8^+$ thymocytes ex vivo developed from indicated genotypes of $CD4^-CD8^-$ thymocytes placed on the OP9-DL4 stroma cells for 3 days ($n = 3$ per genotype). The number indicates the percentage of cells in the gated area throughout. Right: Percentage of $CD4^+CD8^+$ and $CD4^+$ cells. (**B**) Representative flow cytometric analysis (left) of $CD4^+$ and $CD8^+$ thymocytes ex vivo developed from sorted $ROR\gamma t^{-/-}CD4^-CD8^-$ thymocytes transduced with retrovirus expressing GFP alone (EV) or with RORγt, and cultured on OP9-DL4 stroma cells for 3 days ($n = 3$ per genotype). Right: Percentage of $CD4^+CD8^+$ + $CD4^+$ cells. (**C**) Representative flow cytometric analysis of IL-17A (left) and percentage of IL-17A$^+$ cells (right) among indicated genotypes of $CD4^+$ T cells transduced with retrovirus expressing GFP alone (EV) or with RORγt and polarized under T_H17 conditions for 3 days ($n = 3$ per genotype). (**D**) Mean clinical EAE score of $Rag1^{-/-}$ mice adoptively transferred with same number of Tg^{Tcr2D2} or $ROR\gamma t^{-/-}/Tg^{Tcr2D2}$ $CD4^+$ T cells transduced with retrovirus expressing GFP alone (EV) or with RORγt and polarized under T_H17 conditions for 3 days. Bars are means ± SE. ***$P < 0.001$ (two-tailed Student's t test).
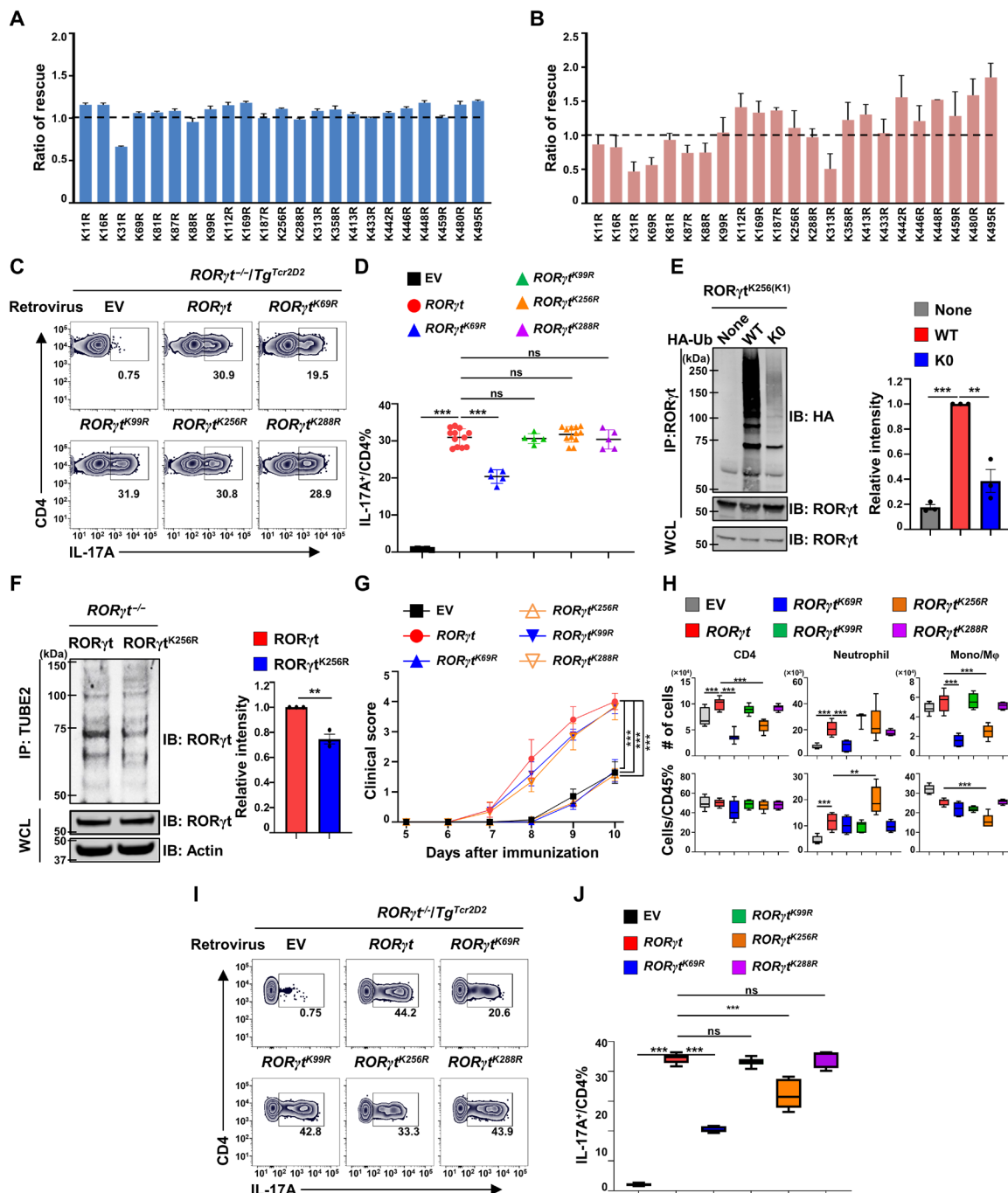
Fig. 2. RORγt-K256, a ubiquitination site, is critical for the effector function but not the differentiation of T_H17 cells. (**A**) The ratio of rescued thymocyte development of $RORγt^{-/-}CD4^-CD8^-$ by indicated RORγt K-R mutants relative to that by WT RORγt (1 = 100%). (**B**) Ratio of rescued T_H17 differentiation of $RORγt^{-/-}CD4^+$ T cells by indicated RORγt K-R mutants relative to WT RORγt (1 = 100%). (**C**) Flow cytometric analysis of IL-17A^+ cells among $RORγt^{-/-}$ CD4^− T cells transduced with retroviruses expressing GFP alone (EV) or indicated RORγt mutants and subsequently polarized for 3 days under T_H17 conditions. (**D**) Percentages of IL-17A^+ cells rescued by indicated RORγt mutants shown in (C) (n = 5 to 12). (**E**) Immunoblot (IB) of ubiquitinated (Ub) RORγt^{K256(K1)} immunoprecipitated (IP) from human embryonic kidney (HEK) 293T cells expressing RORγt^{K256(K1)} alone (none) or together with hemagglutinin (HA)–tagged WT or mutated ubiquitin (K0, all K mutated to R). WCL, whole-cell lysates. (**F**) Immunoblot of ubiquitinated WT RORγt or RORγt^{K256R} (only K256 mutated to R) enriched by Tandem Ubiquitin Binding Entities 2 (TUBE2) from $RORγt^{-/-}$ T_H17 cells expressing indicated RORγt type. (**G**) Mean clinical score of $Rag1^{-/-}$ mice adoptively transferred with sorted $RORγt^{-/-}/Tg^{Tcr2D2}$ T_H17 cells expressing GFP alone (EV) or with indicated RORγt (n = 5 to 7 mice per group). (**H**) Total number and percentage of indicated immune cells recovered from the CNS of EAE-induced mice from (G). (**I**) Flow cytometric analysis of IL-17A^+ cells among CD4^+ T cells recovered from the CNS of EAE-induced mice shown in (G). (H and I) Box plots show median (central line), maximum, minimum (box ends), and outliers (extended lines). *P < 0.05; **P < 0.01; ***P < 0.001; ns, not significant (P > 0.05); two-tailed Student's t test.

suggesting that RORγt uses very different mechanisms to regulate the function of thymocytes and T_H17 cells.

To separate RORγt function in T_H17 differentiation versus effector T_H17 cells, we focused on mutants that did not perturb T_H17 differentiation and thymocyte development, such as K99R, K256R, and K288R (Fig. 2, A to D). K256 was identified as a prominent ubiquitination site by mass spectrometry analysis of immunoprecipitated RORγt (fig. S2A). To validate the K256 ubiquitination site, we generated a RORγt mutant with all K mutated to R except K256 (RORγt$^{K256(K1)}$) so that only K256 can be ubiquitinated. In the presence of WT ubiquitin, RORγt$^{K256(K1)}$ was ubiquitinated, whereas the ubiquitination signals were absent in the presence of a mutant ubiquitin that had all K mutated to R (K0) so that it cannot be attached to the substrates (Fig. 2E). We next used a RORγt mutant carrying a single K256 to R mutation (RORγt^{K256R}) that cannot be ubiquitinated only at the K256 site. WT RORγt or RORγt^{K256R} was then expressed in $RORγt^{-/-}$ T cells under T_H17-polarizing conditions. Ubiquitinated RORγt was readily detected in T_H17 cells (Fig. 2F). Compared to the WT RORγt, RORγt^{K256R} had obviously reduced ubiquitination signals. RORγt-K256 is thus ubiquitinated in T_H17 cells.

Next, we tested the effector function of T_H17 cells in the induction of EAE. As described above (Fig. 1D), in vitro–differentiated $RORγt^{-/-}/Tg^{Tcr2D2}$ T_H17 cells expressing exogenous RORγt, RORγt^{K99R}, and RORγt^{K288R} induced severe EAE after adoptive transfer into $Rag1^{-/-}$ recipients (Fig. 2G), suggesting that K99R and K288R do not affect the effector function of T_H17 cells in the induction of EAE, whereas RORγt^{K256R}-expressing $RORγt^{-/-}/Tg^{Tcr2D2}$ T_H17 cells induced greatly impaired EAE. RORγt^{K69R} also induced impaired EAE, as we previously observed because of reduced T_H17 differentiation (8). There was no difference in the proliferation of the $RORγt^{-/-}/Tg^{Tcr2D2}$ cells expressing various RORγt (fig. S2B). The central nervous system (CNS) immune cell infiltrate was also analyzed (Fig. 2H and fig. S2C for gating strategy). Consistent with the impaired EAE, the total number of CD4$^+$ T cells and monocytes/macrophages in the CNS was significantly reduced in recipients with RORγt^{K256R} or RORγt^{K69R} mutants, indicating reduced inflammation. In addition, recipients with RORγt^{K256R} and RORγt^{K69R} cells also showed reduced infiltrate IL-17A$^+$ cells in the CNS (Fig. 2I and fig. S2D for gating strategy), whereas not obvious changes in interferon-γ–positive (IFN-γ$^+$) T_H1 cells from recipients with RORγt^{K256R} compared to that with WT RORγt were observed (fig. S2, E and F). Therefore, the RORγt-K256 ubiquitination site, although dispensable for T_H17 differentiation, is required for the effector function of T_H17 cells in the pathogenesis of EAE.

RORγt-K256R mutation does not affect RORγt-dependent development of thymocytes and lymph nodes

To investigate the function of RORγt-K256 ubiquitination in vivo, we generated homozygous mice for RORγt^{K256R} ($RORγt^{K256R/K256R}$) under the control of endogenous $RORγt$ locus (fig. S3A for genetic engineering strategy and fig. S3B for confirming the K256R mutation by sequencing). We first examined RORγt-dependent thymocyte development (18–20, 32). WT RORγt and RORγt^{K256R} had the same expression patterns in thymocytes (Fig. 3A); our gene-targeting strategy thus did not affect RORγt^{K256R} expression. Furthermore, RORγt^{K256R} was as stable as WT RORγt (fig. S3, C to D), suggesting that K256 ubiquitination site does not affect RORγt stability. Thymic cellularity (Fig. 3B) and distribution of different developmental stages of thymocytes, CD4$^-$CD8$^-$ double-negative (DN), CD4$^+$CD8$^+$

double-positive (DP), and CD4$^+$ or CD8$^+$ single-positive thymocytes (Fig. 3C) were comparable between $RORγt^{K256R/K256R}$ and WT mice, which were different from $RORγt^{-/-}$ mice, suggesting normal thymocyte development in $RORγt^{K256R/K256R}$ mice. Furthermore, the percentage of natural killer T (NKT) and γδ T cells in the thymus (Fig. 3, D and E) and spleens (fig. S3, E and F) was equivalent between WT and $RORγt^{K256R/K256R}$ mice. The accelerated CD4$^+$CD8$^+$ thymocyte apoptosis (Fig. 3F and fig. S3G for analysis of apoptotic cells) accounted for the reduced percentage of CD4$^+$CD8$^+$ thymocytes (Fig. 3C) and decreased thymic cellularity (Fig. 3B) in $RORγt^{-/-}$ mice (18), whereas the apoptosis of CD4$^+$CD8$^+$ thymocytes from $RORγt^{K256R/K256R}$ mice was the same as that of the WT mice (Fig. 3F). In addition, thymocytes from $RORγt^{-/-}$ mice had a higher percentage of cells with >2N of DNA (Fig. 3G), indicating more cells in the DNA synthesis phase of the cell cycle (18), while thymocytes from $RORγt^{K256R/K256R}$ mice did not show an increased percentage of the cells in the DNA synthesis phase compared to the WT mice. Therefore, RORγt-K256R mutation does not affect RORγt function in thymocyte development. Furthermore, unlike $RORγt^{-/-}$ mice that lack all the peripheral lymph nodes (18), $RORγt^{K256R/K256R}$ mice developed lymph nodes including inguinal lymph nodes (Fig. 3H) and Peyer's patches (Fig. 3I), same as the WT mice. Together, prevention of RORγt-K256 ubiquitination does not affect the development of thymocytes and lymph nodes.

$RORγt^{K256R/K256R}$ mice have normal T_H17 differentiation but develop impaired T_H17-dependent EAE

Upon maturation in the thymus, T cells migrate to the periphery to mediate immune responses. $RORγt^{K256R/K256R}$ and WT mice had comparable splenocytes (fig. S4A), CD4$^+$, CD8$^+$ (fig. S4B), CD62L^{hi}CD44^{lo} naïve, and CD62L^{lo}CD44^{hi} memory-like T cell counts (fig. S4, C to D). We next examined T_H17 differentiation using a GFP reporter mouse line of IL-17 ($Il17a^{GFP}$). We confirmed that in vitro–differentiated $RORγt^{K256R/K256R}$ T_H17 cells showed comparable RORγt (Fig. 4A) and IL-17 (Fig. 4B) expression compared to WT cells, consistent with the notion that RORγt-K256R mutation does affect T_H17 differentiation (Fig. 2, B and D). In addition, $RORγt^{K256R/K256R}$ mice showed a normal percentage of splenic regulatory T cells (T_{regs}) (fig. S4E) and normal differentiation of T_{regs} from naïve CD4$^+$ T cells (fig. S4F). To test whether RORγt-K256R affects the effector function of T_H17 cells responsible for the induction of EAE, we induced EAE by immunization with MOG$_{35–55}$ peptide. Before immunization, there were almost no T_H17 cells detected in the spleens from WT and $RORγt^{K256R/K256R}$ mice (Fig. 4C, top). Six days after immunization, equivalent T_H17 (fig. S4, G and H) as well as T_H1 (fig. S4, I to J) cells were induced in spleens (fig. S4, G and I) and lymph nodes (fig. S4, H and J) of WT and $RORγt^{K256R/K256R}$ mice. Again, on day 12 after immunization, when EAE symptoms started to develop, the percentage of T_H17 cells still showed no obvious difference in the spleens of WT and $RORγt^{K256R/K256R}$ mice (Fig. 4C, bottom), confirming that RORγt-K256R does not affect the generation of T_H17 cells in vivo. However, compared to WT mice, $RORγt^{K256R/K256R}$ mice developed greatly impaired EAE (Fig. 4D), supporting impaired $RORγt^{K256R/K256R}$ T_H17 effector function. Consistently, adoptive transfer of in vitro–differentiated $RORγt^{K256R/K256R}$ T_H17 cells also induced less severe EAE in $Rag1^{-/-}$ recipients compared to that induced by WT T_H17 cells (fig. S4K). In addition, impaired EAE induction was associated with reduced immune cell infiltrate including CD4$^+$, CD8$^+$, B cells, and monocytes in the CNS of $RORγt^{K256R/K256R}$ mice, although no
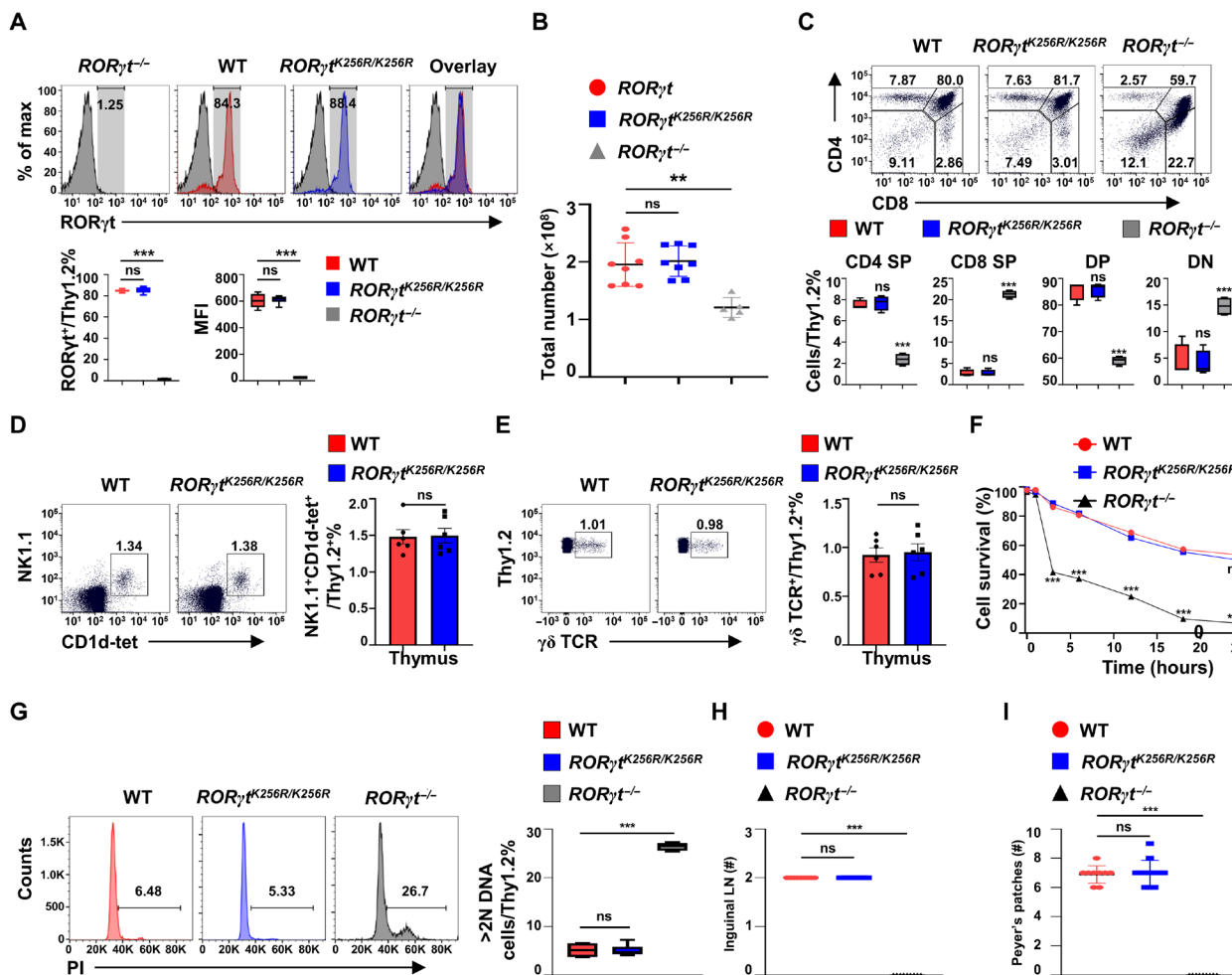
Fig. 3. RORγt-K256R mutation does not affect RORγt-dependent development of thymocytes and lymph nodes. (**A**) Flow cytometric analysis of RORγt in thymocytes obtained from indicated mice ($n = 5$ to 8). MFI, mean fluorescence intensity. (**B**) Total thymocyte numbers of the indicated mice ($n = 5$ to 8). The graph shows mean ± SD. (**C**) Flow cytometric analysis of CD4 and CD8 on thymocytes from indicated mice ($n = 4$ per genotype). (**D**) Representative flow cytometric analysis of NKT cells ($n = 4$) from the thymus of the indicated mice. (**E**) Representative flow cytometric analysis of γδ T cells ($n = 4$) from the thymus of the indicated mice. (**F**) Flow cytometric analysis of the survival of DP thymocytes cultured in vitro for the indicated time ($n = 4$ per genotype). (**G**) Representative flow cytometric analysis of DNA content of indicated thymocytes stained by propidium iodide (PI) ($n = 4$ to 6 per genotype). (**H** and **I**) Number of inguinal lymph nodes (LN) (H) and Peyer's patches (I) in the indicated mice ($n = 9$ to 12 per genotype). **$P < 0.01$; ***$P < 0.001$ (two-tailed t test). (A, C, E, F, and G) Box plots or scatter plots show median (central line), maximum, minimum (box ends), and outliers (extended lines).

obvious changes were observed in neutrophil numbers (Fig. 4E and fig. S4L for gating strategy). Further analysis of CNS lymphocyte infiltrate in the $RORγt^{K256R/K256R}$ mice showed a decreased percentage of IL-17A$^+$CD4$^+$ cells (Fig. 4F), particularly pathogenic IL-17A$^+$ granulocyte-macrophage colony-stimulating factor–positive (GM-CSF$^+$) cells that play an important role in EAE development (Fig. 4, G and H, and fig. S4M for gating strategy) (2, 3). These results suggest that RORγt-K256R mutation, which prevents the ubiquitination, impairs the effector function but not the differentiation of T$_H$17 cells responsible for the pathogenesis of EAE.

RORγt-K256R impairs the pathways critical for the pathogenesis of EAE but not for the T$_H$17 differentiation

To understand the mechanisms responsible for the RORγt-K256R mutation–disrupted effector function of T$_H$17 cells responsible for

EAE, GFP$^+$ T$_H$17 cells derived from WT and $RORγt^{K256R/K256R}$/ IL-17^{GFP} CD4$^+$ T cells were sorted to high purity (>98%) (fig. S5A for gating strategy) and subjected to RNA sequencing (RNA-seq) analysis. On the basis of the computational principal components analysis, the six RNA-seq samples were divided into two groups: WT and $RORγt^{K256R/K256R}$ T$_H$17 cells (fig. S5B), indicating reproducible gene expression patterns within each group and thus the high quality of RNA-seq results. We identified 1375 differentially expressed genes (DEGs) [$P < 0.05$ and fold change (FC) > 1.5], with 943 up-regulated and 432 down-regulated genes, between WT and $RORγt^{K256R/K256R}$ T$_H$17 cells (Fig. 5A, fig. S5C, and tables S2 and S3). Subjection of DEGs to pathway analysis did not find significant changes in the T$_H$17 differentiation pathway (Fig. 5, B and C) between WT and $RORγt^{K256R/K256R}$ cells, confirming that RORγt-K256R mutation does not affect T$_H$17 differentiation. Down-regulated pathways in $RORγt^{K256R/K256R}$ cells include IL-23 signaling (Fig. 5, B and D) and glycolysis pathways
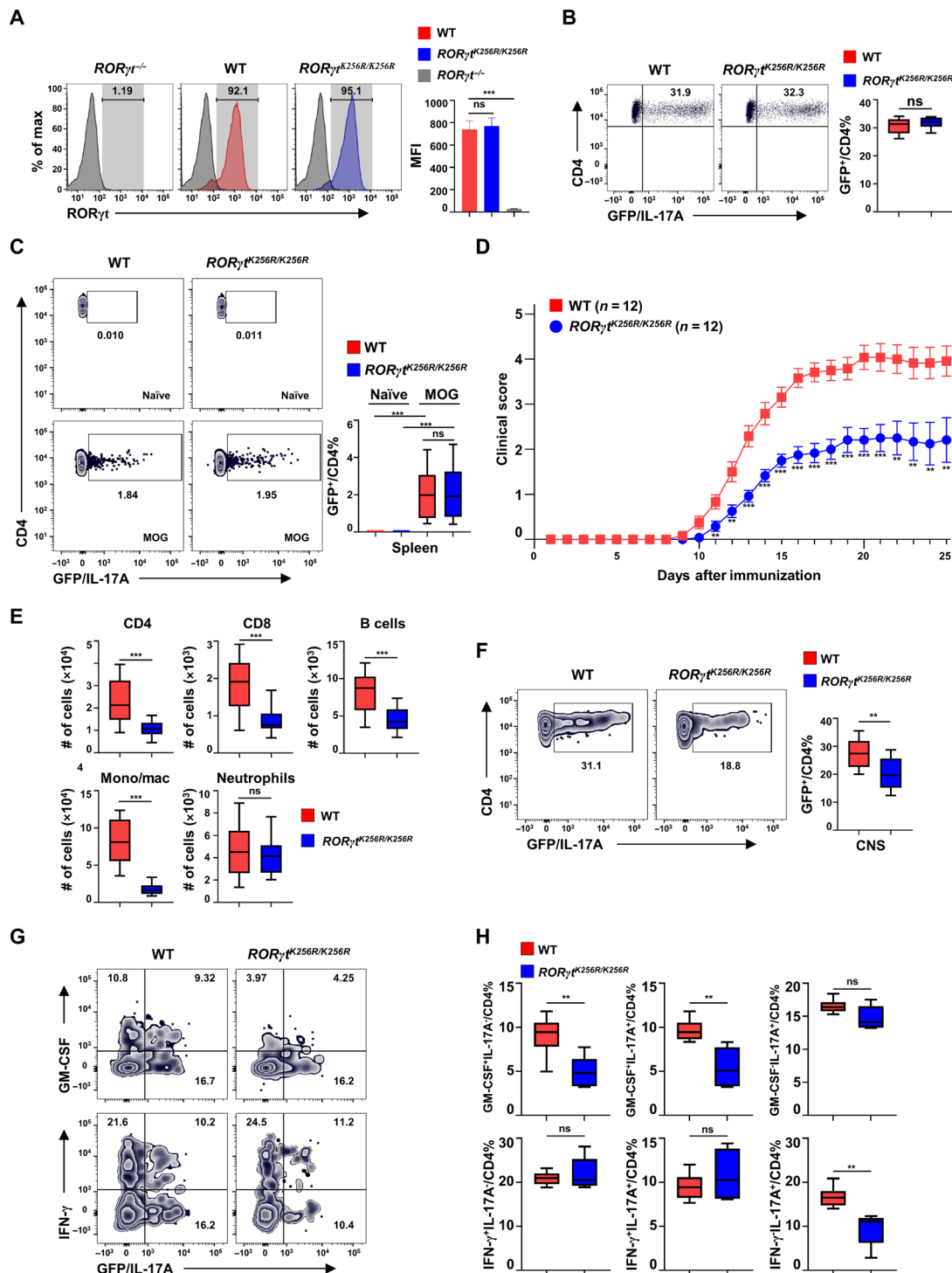
Fig. 4. $ROR\gamma t^{K256R/K256R}$ mice have normal T_H17 differentiation but develop impaired T_H17-dependent EAE. (**A**) Flow cytometric analysis of RORγt in WT and $ROR\gamma t^{K256R/K256R}$ CD4$^+$ T cells polarized for 3 days under T_H17 conditions ($n = 4$ to 6 per genotype). Bars are means ± SEM. (**B**) Flow cytometric analysis of GFP$^+$ (IL-17A$^+$) cells among CD4$^+$ T cells from indicated genotypes of cells differentiated under T_H17 conditions as described in (A) ($n = 4$ per genotype). (**C**) Representative flow cytometric analysis of IL-17A$^+$ cells among CD4$^+$ T cells in the spleen of indicated genotype of mice either before (naïve) or 12 days after MOG$_{35-55}$ immunization ($n = 4$). (**D**) Mean clinical score of indicated mice different days after MOG$_{35-55}$ immunization. Bars are means ± SEM. (**E**) Number of indicated immune cells recovered from the CNS of indicated EAE-induced mice from (D). (**F**) Representative flow cytometric analysis of GFP$^+$ (IL-17A$^+$) among CD4$^+$ T cell infiltrate to the CNS of indicated mice shown in (D) ($n = 10$ per genotype). (**G**) Representative flow cytometric analysis of GM-CSF or IFN-γ expression in the lymphocyte infiltrated to the CNS of indicated mice shown in (D). (**H**) Quantification of GM-CSF$^+$/CD4$^+$ % and IFN-γ^+/CD4$^+$ % cells in the CNS ($n = 5$ per genotype). **$P < 0.01$; ***$P < 0.001$ (two-tailed t test). (E, F, and H) Box plots: Median (central line), maximum, minimum (box ends), and outliers (extended lines).
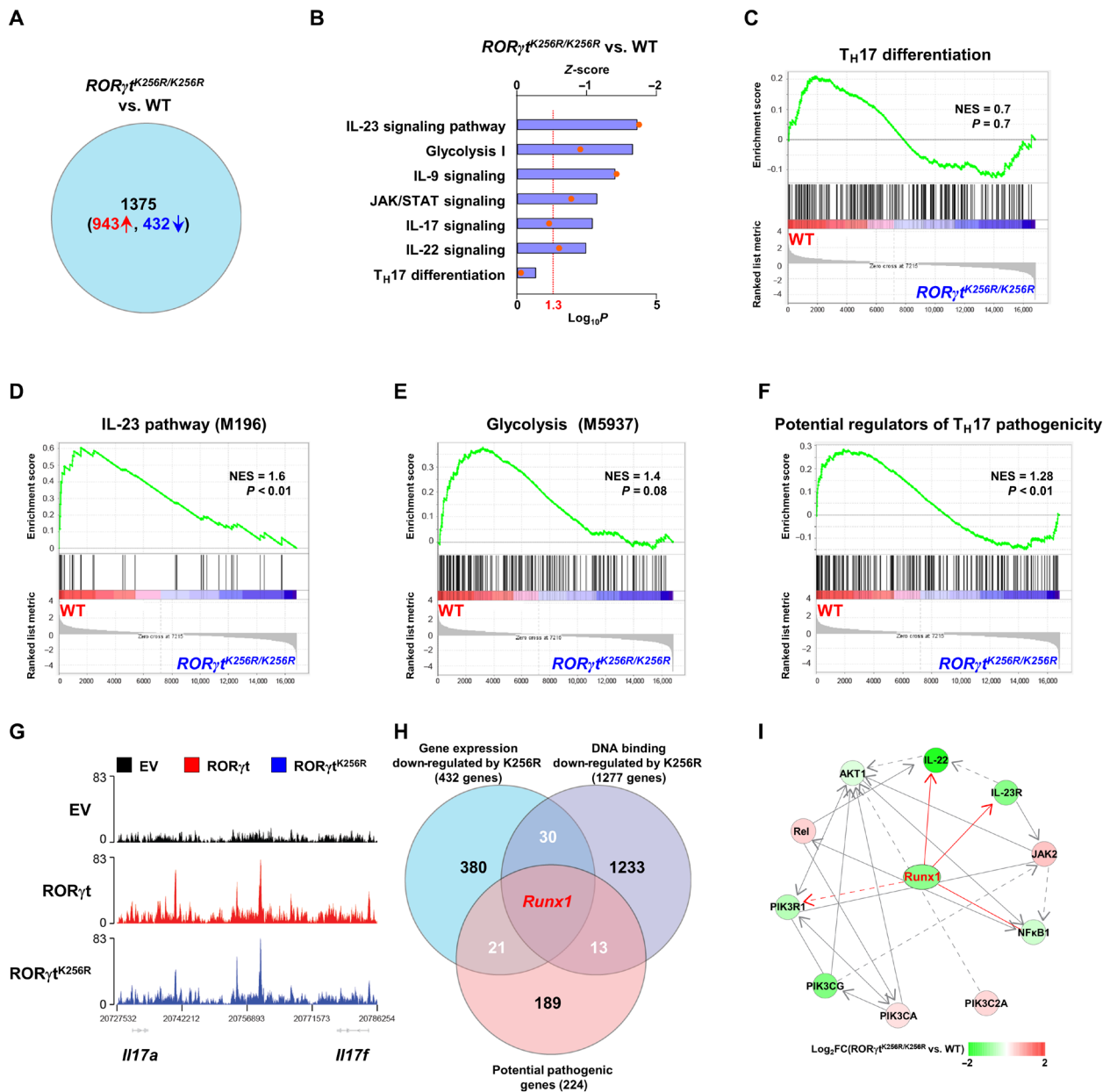
Fig. 5. RORγt-K256R impairs the pathways critical for the pathogenesis of EAE but not for the T_H17 differentiation. (A to F) Computation analysis of RNA-seq data obtained from GFP⁺/(IL-17A⁺) WT and *RORγt^K256R/K256R* CD4⁺ T cells polarized under T_H17 conditions. (A) The number of DEGs (black) including up-regulated (red) and down-regulated (blue) genes with a cutoff at *P* value of <0.05 and FC > 1.5. (B) Ingenuity pathway analysis (IPA) canonical signaling pathway analysis of down-regulated pathways (*z*-score < 0) in *RORγt^K256R/K256R* versus WT T_H17 cells. The dots denote *P* value, the vertical dotted line marks *P* value of 0.05 (log_10*P* = 1.3). JAK, Janus kinase; STAT, signal transducer and activator of transcription. (C to F) GSEA plots showing the enrichment of genes critical for T_H17 differentiation (C), IL-23 signaling (D), glycolysis (E), and pathogenesis of T_H17-mediated EAE (F) between *RORγt^K256R/K256R* versus WT T_H17 cells. NES, normalized enrichment score. Gene sets were derived from the molecular signaling database (MSigDB) for (C) to (E) and the previous report for (F) (*35*). (G) ChIP-seq analysis of RORγt DNA-binding peaks at the *Il17a* and *Il17f* loci in *RORγt^−/−* T_H17 cells expressing indicated RORγt. (H) Venn diagram of gene overlapping among 432 down-regulated genes in *RORγt^K256R/K256R* T_H17 cells, 1277 genes with decreased RORγt^K256R-binding activity, and 224 T_H17 genes critical for the pathogenesis of EAE. (I) Protein-protein network analysis of differentially expressed regulators critical for the IL-23 signaling pathway between *RORγt^K256R/K256R* versus WT T_H17 cells. Genes critical for IL-23 signaling pathway were customized on the basis of IPA-curated pathways.

(Fig. 5, B and E); both play important roles in the pathogenesis of EAE (*33, 34*). In addition, inflammatory cytokines such as IL-9, IL-17, and IL-22 signaling pathways were also down-regulated, likely reflecting a reduced ability to induce inflammation responsible for the tissue damages. We next subjected DEGs to gene set enrichment analysis (GSEA) using the gene set specifically expressed in T_H17 cells responsible for the development of pathogenic EAE (fig. S5D) (*35*) and found that *RORγt^K256R/K256R* T_H17 cells had significantly reduced enrichment of the genes important for the pathogenesis of EAE when compared to the WT T_H17 cells (Fig. 5F). This result is

consistent with the impaired EAE observed in $ROR\gamma t^{K256R/K256R}$ mice. To determine the DEGs that are directly regulated by RORγt, we performed chromatin immunoprecipitation sequencing (ChIP-seq) analysis to detect genome-wide RORγt occupancy. ChIP-seq analysis in T_H17 cells revealed obvious RORγt-binding peaks at *Il17a* and *Il17f* loci (Fig. 5G), consistent with published results (*8, 36*). RORγt^{K256R}-binding peaks at the *Il17a and Il17f* loci were comparable to that of WT RORγt, supporting that K256R did not affect RORγt binding to *Il17* gene and thus its expression. Using our RNA-seq and ChIP-seq data, we cross-examined genes that were down-regulated in $ROR\gamma t^{K256R/K256R}$ T_H17 cells with the genes that had reduced RORγt^{K256R}-binding signals (see table S4 for the full list), identifying 31 genes (Fig. 5H). These 31 genes are considered directly regulated by RORγt, and their reduced expression in $ROR\gamma t^{K256R/K256R}$ T_H17 cells is likely due to reduced RORγt^{K256R} binding and activating their expression. The 31 genes were then cross-examined with the gene set specifically expressed in T_H17 cells and responsible for the pathogenesis of EAE (fig. S5D) (*35*) and identified *Runx1* (Fig. 5H). Furthermore, *Runx1* was found to be a core regulator for the IL-23 signaling pathway that was down-regulated in $ROR\gamma t^{K256R/K256R}$ T_H17 cells by a protein-protein interaction network analysis (Fig. 5I), indicating that down-regulated IL-23 signaling pathway is likely due to down-regulated *Runx1* expression. Therefore, computational analysis of the transcriptome is consistent with the phenotypes observed in $ROR\gamma t^{K256R/K256R}$ mice that RORγt-K256R mutation does not affect T_H17 differentiation but impairs the effector function of T_H17 cells responsible for the development of EAE. *Runx1* is thus a possible RORγt-regulated gene that is down-regulated in $ROR\gamma t^{K256R/K256R}$ T_H17 cells and responsible for the observed defective effector function of $ROR\gamma t^{K256R/K256R}$ T_H17 cells in the induction of EAE.

RORγt-K256R mutation impairs RORγt to bind and activate *Runx1* gene critical for EAE development

Our computational analysis identified *Runx1* as a potential gene responsible for impaired effector function of $ROR\gamma t^{K256R/K256R}$ T_H17 cells, because (i) *Runx1* was down-regulated in $ROR\gamma t^{K256R/K256R}$/ Tg^{Tcr2D2} T_H17 cells, which was also confirmed by individual quantitative polymerase chain reaction (qPCR) analysis (Fig. 6A); (ii) three prominent RORγt-binding peaks close to the transcription start site of *Runx1* gene were identified by ChIP-seq analysis (Fig. 6B), and RORγt^{K256R} binding signals at those peaks were substantially decreased (Fig. 6, B and C). RORγt-binding sites were identified within the peak region by sequencing analysis (fig. S6A). Furthermore, individual ChIP assays also confirmed RORγt binding to the peak region, whereas RORγt^{K256R}-binding signals to this region were greatly decreased (Fig. 6D), which correlates to the decreased levels of *Runx1* mRNA in $ROR\gamma t^{K256R/K256R}$ T_H17 cells (Fig. 6A); (iii) *Runx1* was a gene expressed in T_H17 cells and responsible for the pathogenesis of EAE, as deletion of *Runx1* impairs the EAE development (*35, 37*). To determine the effects of decreased RORγt^{K256R}-binding peak signals on *Runx1* gene transcription, we cloned the DNA fragment covering the region with two potential RORγt-binding sites (fig. S6A) to a luciferase reporter gene (pGL3) driven by a basic thymidine kinase (TK) promoter. The reporter activity was greatly stimulated by WT RORγt but not as much by RORγt^{K256R} (Fig. 6E). Therefore, reduced RORγt^{K256R} binding to the *Runx1* gene correlates well with the reduced ability of RORγt^{K256R} to stimulate *Runx1* gene expression. In contrast, WT RORγt and RORγt^{K256R} equivalently stimulated IL-17 promoter-luciferase report activity, which correlates with the equivalent

binding of RORγt and RORγt^{K256R} to and activation of the *Il17* gene (Figs. 4B and 5G). To further determine whether identified RORγt-binding peaks are important for the expression of endogenous *Runx1* gene, the region containing the RORγt-binding peaks was deleted using CRISPR-Cas9 with two guiding RNAs (ΔRgn1) in CD4$^+$ T from mice expressing Cas9 (fig. S6A). At the same time, we used a non-targeting control (NTC) and a deleted adjacent region (ΔRgn2) as negative controls, whereas deleted *Runx1* gene itself as a positive control (ΔRunx1) (fig. S6B for gating strategy for detecting Runx1 expression after deletion). Deletion of the *Runx1* gene prevented Runx1 expression [Fig. 6F and fig. S6C for mean fluorescence intensity (MFI) of Runx1], demonstrating a successful deletion strategy with CRISPR-Cas9. Furthermore, deletion of the RORγt-binding region, but not the adjacent region or NTC, greatly reduced expression of Runx1, strongly indicating the critical function of the RORγt-binding region in the stimulation of *Runx1* expression. Together with the results that RORγt^{K256R} had decreased binding signals to *Runx1* (Fig. 6, B to D), these results suggest that reduced *Runx1* expression in $ROR\gamma t^{K256R/K256R}$ T_H17 cells is due to impaired RORγt^{K256R}-binding and activating *Runx1* gene expression. To determine whether the reduced level of *Runx1* in $ROR\gamma t^{K256R/K256R}$ cells is responsible for the impaired development of EAE, we force-expressed *Runx1* in $ROR\gamma t^{K256R/K256R}$/$Tg^{Tcr2D2}$ CD4$^+$ T cells (Fig. 6G) and adoptively transferred them to $Rag1^{-/-}$ mice to induce EAE (Fig. 6H). Forced expression of *Runx1* significantly enhanced $ROR\gamma t^{K256R/K256R}$/$Tg^{Tcr2D2}$ CD4$^+$ T cell function in the induction of EAE comparable to that of WT Tg^{Tcr2D2} T cells, which was also confirmed by increased infiltration of CD4$^+$ T cells to the CNS (Fig. 6I). Furthermore, the percentage of pathogenic IL-17$^+$GM-CSF$^+$ and IL-17$^+$IFN-γ$^+$ cells in CNS was reduced in $Rag1^{-/-}$ mice transferred with $ROR\gamma t^{K256R/K256R}$/$Tg^{Tcr2D2}$ CD4$^+$ T cells compared to that transferred with WT Tg^{Tcr2D2} T cells but restored to WT levels in $ROR\gamma t^{K256R/K256R}$/$Tg^{Tcr2D2}$ CD4$^+$ T cells expressing *Runx1* (Fig. 6J), consistent with rescuing the effector function of $ROR\gamma t^{K256R/K256R}$ T cells by expressing *Runx1*. Collectively, our results demonstrated that the ubiquitination site of RORγt-K256, which is not essential for T_H17 differentiation, regulates the effector function of T_H17 cells required for inducing EAE via up-regulating *Runx1*. By decoupling the function of RORγt in the differentiation and effector function of T_H17 cells, we demonstrated that RORγt also regulates the effector function of T_H17 cells.

DISCUSSION

The transcription factor RORγt, which is encoded by gene *Rorc*, is well known for instructing the differentiation of T_H17 cells. Activation of naïve T cells in the presence of TGF-β, IL-6, and/or IL-23 is sufficient to up-regulate RORγt, which instructs the differentiation into T_H17 cells (*14, 38–41*). The hallmark of T_H17 differentiation is the activation and expression of IL-17. RORγt directly binds to *Il17a* and *Il17f* gene loci to stimulate their expression (*8, 36*), which explains the essential function of RORγt in the differentiation of IL-17–producing T_H17 cells. Differentiated T_H17 cells are able to induce tissue inflammation involved in the pathogenesis of autoimmune diseases, including psoriasis, inflammatory bowel disease, and multiple sclerosis (*2, 3, 14*). Previous studies using $ROR\gamma t^{-/-}$ mice demonstrated the essential function of RORγt in T_H17 cell–mediated autoimmunity such as EAE (*7, 9*). $ROR\gamma t^{-/-}$ mice are resistant to EAE and other T_H17-mediated autoimmunity, which is due to the lack of RORγt-dependent generation of T_H17 cells. The question remains
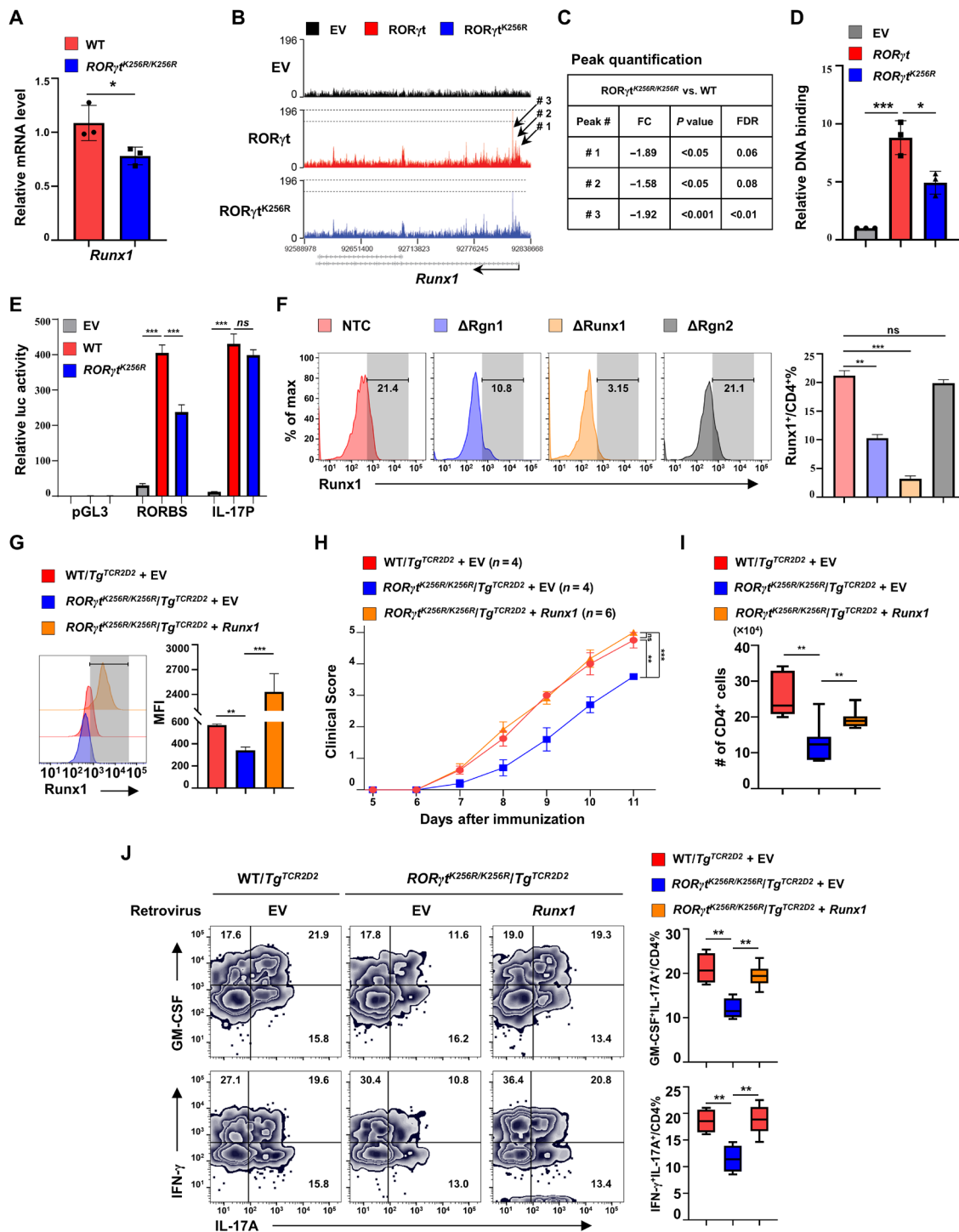
Fig. 6. RORγt-K256R mutation impairs RORγt to bind and activate *Runx1* gene critical for EAE development. (A) qPCR of *Runx1* mRNA in indicated genotypes of T_H17 cells (*n* = 3). Bars are means ± SEM. (**B**) ChIP-seq analysis of RORγt DNA-binding peaks at the *Runx1* locus in *RORγt*^−/−^ T_H17 cells transduced with indicated vectors. (**C**) FC of RORγt-binding peaks indicated in (B). FDR, false discovery rate. (**D**) ChIP analysis of RORγt-binding signals at the *Runx1* gene locus shown in (B) (*n* = 3). Bars are means ± SEM. (**E**) Luciferase (luc) activity from HEK 293T cells transfected with a pGL3 basic luciferase vector, a luciferase reporter with RORγt-binding sites (RORBS)–containing DNA fragment cloned from *Runx1* locus and a basic TK promoter or IL-17 promoter (IL-17P) luciferase reporter under indicated conditions. (**F**) Flow cytometric analysis of Runx1 among GFP^+(Cas9^+) T_H17 cells retrovirally transduced with indicated single-guide RNAs (*n* = 4). (**G**) Flow cytometric analysis of Runx1 among indicated genotypes of T_H17 cells retrovirally transduced with GFP alone (EV) or together with Runx1 (*n* = 3). (**H**) Mean clinical score of *Rag1*^−/−^ mice adoptively transferred with indicated genotypes of T_H17 cells expressing GFP alone or with Runx1 shown in (G). (**I**) Number of infiltrating CD4^+ T cells recovered from the CNS of the EAE-induced mice shown in (H). (**J**) Flow cytometric analysis of GM-CSF, IFN-γ, and IL-17A in CD4^+ T cells recovered from the CNS of EAE-induced mice shown in (H). *$P < 0.05$; **$P < 0.01$; ***$P < 0.001$ (two-tailed *t* test). (I and J) Box plot: Median (central line), maximum, minimum (box ends), and outliers (extended lines).

whether RORγt plays a role in the effector function of T_H17 cells involved in autoimmunity. The mutation RORγt^{K256R} we identified at the ubiquitination site does not affect the generation of IL-17– producing T_H17 cells but impairs the effector function of T_H17 cells in the induction of EAE. Further, RORγt$^{K256R/K256R}$ mice have normal T_H17 differentiation both in vitro and in vivo but have greatly impaired T_H17 immune responses that led to EAE. In addition, RORγt$^{K256R/K256R}$ mice have normal RORγt-dependent thymocyte development and lymph node genesis including Peyer's patches. This study thus reveals a previously unidentified and essential RORγt function in effector T_H17 cells in addition to T_H17 differentiation. This study informs the development of RORγt-based therapies that specifically target the effector function of T_H17 cells responsible for the pathogenesis of autoimmunity. This will have a significant impact on the clinical treatment of T_H17-mediated autoimmunity, as usually medical treatment is performed after a diagnosis of autoimmune diseases resulting from the effector function of already developed T_H17 cells.

Runx1 is a transcription factor known to regulate hematopoiesis (*42–44*) and oncogenesis (*45*). *Runx1* was reported to play a role in T_H17 cells. Particularly relevant to T_H17 cells involved in the pathogenesis of EAE, *Runx1* has been shown to be up-regulated in T_H17 cells and work together with T-bet to stimulate IFN-γ expression that is believed to be responsible for the induction of EAE (*37*). However, it is not clear how *Runx1* is up-regulated in T_H17 cells. Our results demonstrate that *Runx1* expression is stimulated by RORγt, as RORγt-binding peaks were detected by ChIP-seq on the promoter region of the *Runx1* gene. The conserved RORγt-binding sequence was identified within the detected peaks, and the deletion of the DNA fragment containing the RORγt-binding site greatly reduced *Runx1* expression. Moreover, RORγt^{K256R} has reduced binding signals at the RORγt-binding region, which correlates with the impaired ability of RORγt^{K256R} in stimulating a luciferase reporter gene driven by the RORγt-binding region identified in the *Runx1* locus. These results demonstrate the mechanisms for how RORγt regulates the effector function of T_H17 cells via up-regulating *Runx1* expression and why RORγt-K256R mutation impairs the effector function of T_H17 cells. An in vitro study showed that *Runx1* can stimulate RORγt expression, which is, however, inhibited by T-bet (*46*). Because T-bet is required for IFN-γ expression, this seems to suggest that T-bet and RORγt inhibit each other. In addition, *Runx1* has been shown to be required for forkhead box P3 (Foxp3) expression (*47*), and *Runx1* is able to stimulate itself expression via an autoregulation mechanism (*48*). The function of *Runx1* is thus complicated and dependent on the microenvironment. In our study, both in vitro and in vivo, we did not find obvious changes in the levels of RORγt expression in RORγt$^{K256R/K256R}$ T_H17 cells that have lower levels of *Runx1*, thus not supporting the role of K256 ubiquitination in the regulation of RORγt and T_H17 differentiation. Furthermore, even forced expression of *Runx1* in RORγt$^{K256R/K256R}$ CD4$^+$ T cells does not affect T_H17 differentiation. Therefore, RORγt-regulated *Runx1* expression does not affect T_H17 differentiation but is required for the effector function of T_H17 cells that mediate pathogenic EAE.

Dysregulated T_H17 cells are often associated with autoimmune diseases such as EAE and psoriasis resulting from a reaction to self-antigens (*49*). In addition to IL-17, IL-23 also plays an important role in T_H17 cell–dependent autoimmune diseases (*1*, *50*) such as EAE and psoriasis (*51*, *52*). Neutralizing antibodies for IL-23 and IL-17 or their receptors are used for the treatment of these autoimmune conditions (*53–55*). Therefore, inhibiting the T_H17 pathway is effective

for treating autoimmune conditions (*52*, *56*). Our results show that the IL-23 signaling pathway is down-regulated in RORγt$^{K256R/K256R}$ T_H17 cells. Further, network analysis supports that *Runx1* is a core regulator for the IL-23 pathway and down-regulated IL-23 pathway thus likely resulting from down-regulated *Runx1*. Therefore, RORγt-regulated *Runx1* seems to control the effector function of T_H17 cells at least partially through regulating the IL-23 pathway known to be critical for T_H17-mediated autoimmunity.

Considering the essential function of RORγt in T_H17 cells, RORγt inhibitors are being developed to treat T_H17-dependent autoimmunity (*5*, *11–13*, *57*). However, these RORγt inhibitors mostly target T_H17 differentiation and RORγt-dependent thymocyte development. Inhibition of RORγt-dependent thymocyte development leads to a high frequency of thymic lymphoma (*8*, *58*, *59*). Our results demonstrate that a posttranslational ubiquitination event can dictate RORγt function in T_H17-dependent responses involved in autoimmunity. However, this ubiquitination event is dispensable for thymocyte development and T_H17 differentiation. Therefore, targeting this RORγt ubiquitination event is a potential treatment for T_H17-dependent autoimmune disease without induction of thymocyte lymphoma. Currently, it remains unknown about the RORγt ubiquitination pathway including the enzymes involved in the ubiquitination of RORγt at K256. Illustrating the detailed mechanisms responsible for ubiquitination of RORγt will facilitate the development of novel treatments that target the RORγt-dependent effector function of T_H17 cells responsible for autoimmunity while minimizing the other toxic effects such as lymphoma.

MATERIALS AND METHODS
Experimental design
The objective of this study was to determine whether RORγt plays a role in effector function of T_H17 cells in addition to its known function in T_H17 differentiation. To achieve this goal, we dissected the function of RORγt with K-R mutations in thymus development, T_H17 differentiation, and induction of EAE. RORγt-K256R mutation did not affect T_H17 differentiation but impaired the effector function of T_H17 cells responsible for inducing EAE, which was also confirmed by the in vivo studies using RORγt$^{K256R/K256R}$ mice. RNA-seq and ChIP-seq assays identified *Runx1* as a direct target of RORγt in the regulation of effector function of T_H17 cells.

Mice
All male and female mice used for experiments were between 6 and 12 weeks old; age-matched littermates were used. The RORγt$^{-/-}$ (*Rorc^{tm1Litt}*, stock no. 007571) mouse strain was described previously (*18*). The RORγt$^{K256R/K256R}$ point-mutated mice were designed and generated by Biocytogen LLC. *Rag1$^{-/-}$* (*Rag1^{tm1Mom}*, stock no. 002216), *Tg^{Tcr2D2}* (Tcra2D2 and Tcrb2D2, stock no. 006912), IL-17A–GFP (*Il17a^{tm1Bcgen}*, stock no. 018472), CRISPR-Cas9– enhanced GFP (EGFP) [*Gt(ROSA)26Sor$^{em1.1(CAG-cas9*,-EGFP)Rsky}$*, stock no. 028555], and C57BL/6J (stock no. 000664) mice were purchased from the Jackson Laboratory. For some assays, the mice were crossed to generate RORγt$^{-/-}$/*Tg^{Tcr2D2}*, RORγt$^{K256R/K256R}$/*Tg^{Tcr2D2}*, and RORγt$^{K256R/K256R}$/*IL-17A-IRES-GFP-KI* mice. All mice were bred at the C57BL/6J background and maintained in a pathogen-free animal facility at City of Hope. All animal experiments were conducted per the protocols approved by the Institutional Animal Care and Use Committee at City of Hope. Statistical tests were not used to predetermine sample

sizes. The sample sizes were chosen on the basis of previous studies of our own and by others in the field (8). The sample sizes are indicated in the figure legends or figures. Allocation of mice to experimental groups was random.

Induction and assessment of EAE

Active EAE was induced and assessed as previously described (8). Briefly, mice were immunized with 200 mg of MOG_{35-55} (Hooke Laboratories) in complete Freund's adjuvant by subcutaneous injection at two dorsal sites at day 0, followed by two intraperitoneal injections of 80 ng of pertussis toxin at days 0 and 1. For passive EAE, $Rag1^{-/-}$ mice were adoptively transferred with 1×10^5 TCR^{MOG}-expressing (Tg^{Tcr2D2}) T_H17 cells that were differentiated under T_H17 polarization condition, followed by an immunization with MOG at 7 days after injection. In certain experiments, WT RORγt cells were virally transduced with retrovirus expressing GFP alone, while $RORγt^{K256R/K256R}$ cells were transduced with retrovirus expressing Runx1 and GFP before in vitro T_H17 differentiation. In other experiments, $RORγt^{-/-}$ cells were transduced with an empty vector or vectors encoding WT RORγt, RORγt^{K87R}, RORγt^{K99R}, RORγt^{K256R}, or RORγt^{K288R}. All transduced cells were sorted for CD4 and GFP expression before adoptive transfer into mice. Severity of EAE was monitored, and a clinical score of 0 to 5 was assigned (30): 0 = no disease, 0.5 = partially limp tail, 1 = paralyzed tail, 2 = hindlimb weakness, 3 = hindlimb paralysis, 4 = hindlimb and forelimb paralysis, and 5 = moribundity and death.

Isolation of naïve CD4$^+$ T cell isolation and in vitro T_H17 differentiation

Murine CD4$^+$ T cells were isolated from spleens by negative selection using the Naive CD4$^+$ T Cell Isolation Kit (Miltenyi Biotec). Suspensions of 4×10^5 cells/ml in RPMI 1640 medium (Corning Inc.) containing 2 mM L-glutamine, 50 μM β-mercaptoethanol, penicillin (100 U/ml), streptomycin (100 mg/ml), and 10% fetal bovine serum (FBS) were activated with hamster anti-CD3 (0.25 μg/ml; 145-2C11, BioLegend) and hamster anti-CD28 (1 μg/ml; 37.51, BioLegend) antibodies overnight in 24-well plates precoated with rabbit anti-hamster immunoglobulin G fraction (0.1 mg/ml; catalog no. 55398, MP Biomedicals). The following T_H17 differentiation was carried out by supplementing to the culture medium mentioned above with TGF-β (2 ng/ml; Miltenyi Biotec), IL-6 (20 ng/ml; Miltenyi Biotec), anti-IL-4 (2 μg/ml; 11B11, BioLegend), and anti–IFN-γ (2 μg/ml; XMG 1.2, BioLegend), and additional IL-23 (20 ng/ml; Miltenyi Biotec) was also added for the induction of pathogenic T_H17 cells.

Retroviral transduction

The retroviral vector murine stem cell virus (MSCV)–internal ribosomal entry site (IRES)–GFP (MIGR1, a gift from W.S. Pear, University of Pennsylvania) was used to clone WT or mutated RORγt. MSCV vector for expressing Runx1 was a gift from I. Taniuchi (RIKEN Center for Integrative Medical Sciences, Japan). Vectors were first transfected to Platinum-E (Cell Biolabs) retroviral packaging cells using BioT transfection reagent (Bioland Scientific), followed by a change of fresh medium at 24 hours. The virus-containing supernatant was collected at 48 and 72 hours, filtered with a 0.45-μm polyvinylidene difluoride (PVDF) syringe filter (Millipore), and used to transduce T cells or stored for future use at −80°C. Transduction of activated CD4$^+$ T was performed by spin infection with viral supernatants (two, 500g, 30°C for 2 hours) in the presence of polybrene

(8 μg/ml; Sigma-Aldrich). After spinning, the plates were incubated at 37°C for 3 hours. The viral supernatant was replaced with fresh culture medium with polarizing cytokines for in vitro differentiation.

CRISPR-Cas9–mediated genomic DNA deletion

Single-guide RNA (sgRNA) of $Runx1$, targeting the exon region (Addgene, library 67988), was cloned to pMSCV-U6sgRNA(Bbs I)-PGKpuro2ABFP (Addgene, 102796) with modification of Bbs I sites (table S1) for using universal primer design through this study. To generate plasmids for the deletion of large fragments of genomic DNA, PCR products of two U6 promoter–sgRNA cassettes and a phosphoglycerate kinase (PGK) promoter–TagBFP cassette were assembled using the Golden Gate assembly method and inserted into the MIGR1 vector with disrupted Bsp MI site. Bbs I sites and newly introduced Bsp MI sites were used for the insertion of gRNAs into each cassette. sgRNAs were delivered to the cells by retroviral transduction. The U6 promoter–driven transcription of sgRNAs in each cassette was confirmed by examining sg$RORγt$ expression in T_H17 cells together with a simultaneously expressed NTC sgRNA in another cassette. Three sgRNAs (sgRNA1, sgRNA2, and sgRNA3; fig. S6A) targeting the sequence of the $Runx1$ gene were designed by using an online tool (CRISPOR, http://crispor.tefor.net/). A simultaneous expression of sgRNA1 with sgRNA2 or sgRNA2 with sgRNA3 in Cas9-expressing cells was designed for deletion of the RORγt binding region (Rgn1) and the adjacent region (Rgn2) without RORγt biding site. sgRNA primers are listed in table S1.

In vitro T cell–development assay

Murine thymocytes from $RORγt^{-/-}$ mice were subjected to fluorescence-activated cell sorting for isolating DN (Thy1.2$^+$CD4$^-$CD8$^-$) cells. Sorted cells at 5×10^5 cells/ml were cultured overnight on an 80% confluent bone marrow-derived stromal cell line (OP9) expressing the delta like canonical Notch ligand 4 (Dll4/DL4) (OP9-DL4) monolayer (a gift from E.V. Rothenberg) in 24-well culture plates with α-modified minimum essential medium (Invitrogen Life Technologies) supplemented with 20% FBS, penicillin-streptomycin (100 U/ml), 2 mM L-glutamine (Invitrogen Life Technologies), and recombinant mouse IL-7 (5 ng/ml; PeproTech). The cells were then transduced with RORγt carrying K/R mutations as described above. Cocultures were maintained for an additional 3 days in the fresh medium containing murine IL-7 (5 ng/ml). Cells were harvested for flow cytometry analysis.

Apoptosis assays

Murine thymocytes were collected by smashing the thymus in a 40-μm cell strainer. Cells were suspended in RPMI 1640 medium supplemented with 10% FBS, 1% penicillin-streptomycin, and 2 mM L-glutamine at 1×10^6 cells/ml and cultured for 0, 3, 6, 12, 18, or 24 hours. Thymocytes were then incubated with anti-Thy1.2 antibody and a fixable LIVE/DEAD near-infrared dye (Thermo Fisher Scientific). After two washes, the cells were stained with 5 μl of phycoerythrin–annexin V in 100 μl of binding buffer containing 0.01 M Hepes (pH 7.4), 0.14 M NaCl, and 2.5 mM CaCl$_2$ for 15 min. An additional 400 μl of binding buffer was added to the suspension before analysis.

RNA-seq and analysis

CD4$^+$ T cells isolated from RORγt^{WT}/IL-17A-GFP$^{+/-}$ and RORγt$^{K256R/K256R}$/IL-17A-GFP$^{+/-}$ mice were differentiated into pathogenic T_H17 cells as described above. RNA was extracted from sorted ~1×10^6 GFP-expressing T_H17 cells (CD4$^+$GFP$^+$) using an RNAeasy mini kit

(QIAGEN). Each group contained three replicates from different mice. Quality control, library preparation, and sequencing were performed at Novogene. The analysis was performed through Partek Flow. Briefly, the sequence reads were aligned to the mouse whole genome (GRCm38) with validation of quality through prealignment and postalignment quality assurance/quality control (QA/QC). Aligned reads were further subjected to quantification using the Partek expectation/maximization (E/M) algorithm and normalization to counts per million with 0.001 added to each. The identification of differentially expressed features was performed through the Partek gene specific analysis (GSA) algorithm that applies multiple statistical models to each gene. Genes with total counts over 30 were considered to be statistically expressed in the cells. The expression values of pathogenic genes were extracted and subjected to ingenuity pathway analysis (IPA), gene set enrichment assay (GSEA), and network analysis.

Chromatin immunoprecipitation sequencing
In vitro–activated (see above) $ROR\gamma t^{-/-}$ CD4$^+$ T cells that were transduced with retroviruses carrying GFP, RORγt-3xFlag/GFP, or RORγt^{K256R}-3xFlag/GFP were used. After T_H17 polarization, 2×10^7 cells were fixed in 1% formaldehyde at room temperature for 10 min to cross-link proteins with chromatin. The reaction was stopped with incubation in glycine for 5 min. Genomic DNA was fragmented with enzyme cocktail (ChIP-IT Express Enzymatic kit, Active Motif) for 10 min as directed. Cell lysates were centrifuged at 15,000 rpm for 10 min to remove debris, and the supernatant was used for immunoprecipitation. An equal amount of DNA was incubated with anti-FLAG (M2, Sigma-Aldrich) overnight, followed by precipitation with protein G agarose beads. Beads complexed with DNA fragments were extensively washed five times, and DNA was eluted, followed by reverse cross-linking. Recovered DNA was subjected to NovaSeq with 51–base pair (bp) paired-end sequencing length. Primers used in reverse-transcription quantitative PCR (RT-qPCR) are listed in table S1. Reads were analyzed using Partek Flow through alignment to the mm10 mouse genome using the Burrow-Wheeler aligner (BWA). Peaks were identified with the model-based analysis of ChIP-seq 2 (MACS2) tool (version 2.1.1) and quantified with a minimum region size of 50 bp.

Flow cytometry
For surface staining, cells isolated from mice or in vitro culture were directly stained with antibodies in phosphate-buffered saline (PBS) with 2% FBS and 1 mM EDTA at 4°C for 15 min. A blocking of Fc receptors with anti-CD16/32 antibody was carried out in case monocytes/macrophages were present. For staining transcription factors, cells were prestained for surface markers, fixed, and permeabilized in TF Fix/Perm buffer (BD Biosciences) at 4°C for 20 min and washed once with TF Perm/Wash buffer. Cells were stained for target proteins (see antibody list below) in the TF Perm/Wash buffer at 4°C for 15 min. For cytokine staining, cells were prestimulated with phorbol 12-myristate 13-acetate (50 ng/ml; Sigma-Aldrich) and ionomycin (750 ng/ml; Sigma-Aldrich) for 3 hours ahead of staining. Meanwhile, GolgiStop (BD Biosciences) was cotreated to block protein transport. In certain experiments, cells were stained with surface markers and/or fixable live/dead dye (Thermo Fisher Scientific). Cells were fixed and permeabilized with CytoFix/CytoPerm buffer (BD Biosciences), followed by staining for cytokines in the Perm/Wash buffer (BD Biosciences) after washing. To measure cell proliferation, either naïve CD4$^+$ T cells or in vitro–differentiated T_H17 cells for adoptive transfer were stained with CellTrace Violet dye (Thermo Fisher Scientific) in PBS (1:5000) at room temperature for 20 min. After washing, naïve CD4$^+$ T cells were subjected to anti-CD3/anti-CD28 stimulation and T_H17 differentiation for measuring in vitro proliferation, and T_H17 cells were sorted out and injected to Rag1$^{-/-}$ mice for measuring hemostatic proliferation at day 3. Subsequent analysis was performed in the BD LSRFortessa flow cytometer.

The following antibodies were used for flow cytometric assay: anti-CD45 (BioLegend, clone 30-F11), anti-CD3 (BioLegend, 145-2C11), CD4 (BioLegend, RM4-5), anti-CD8 (BioLegend, 53-6.7), anti-CD19 (BioLegend, 1D3), anti-lymphocyte antigen 6 complex locus G6D (Ly6G) (BioLegend, 1A8), anti-CD62L (BioLegend, MEL-14), anti-CD44 (BioLegend, IM-7), anti–IFN-γ (BioLegend, XMG-1.2), anti–GM-CSF (BioLegend, MP1-22F9), killer cell lectin-like receptor subfamily B member 1C (Klrb1c/NK1.1) (BioLegend, PK136), anti-CD11b (eBioscience, M1/70), anti-Ly6C (eBioscience, HK1.4), anti-Thy1.2 (eBioscience, 53-1.2), anti–IL-17A (eBioscience, eBio17B7), anti-Runx1 (eBioscience, RXDMC), anti–IL-22 (eBioscience, 1H8PWSR), anti-Foxp3 (eBioscience, FJK-16 s), anti-RORγt (BD Biosiences, Q31-378), and CD1d-tetramer [National Institutes of Health (NIH), PBS-57].

Western blotting
A total 1.5×10^7 T_H17 cells were lysed in radioimmunoprecipitation assay buffer containing 20 mM tris-HCl (pH 7.4), 150 mM NaCl, 1 mM Na$_2$EDTA, 1 mM EGTA, 1% NP-40, 1% sodium deoxycholate, 2.5 mM sodium pyrophosphate, 1 mM β-glycerophosphate, 1 mM Na$_3$VO$_4$, and leupeptin (1 μg/ml). Ubiquitinated proteins were precipitated and enriched with 20 μl of equilibrated agarose-Tandem Ubiquitin Binding Entities 2 (TUBE2) (Lifesensors) at 4°C for 4 hours. Agarose-TUBE2-protein complex were washed with Tris buffered saline containing 0.1% Tween-20 (TBST) and subjected to heating in 2× Laemmli sample buffer (Bio-Rad) with β-mercaptoethanol at 90°C for 5 min. The supernatant containing precipitated proteins was subjected to SDS–polyacrylamide gel electrophoresis, and the protein was transferred to the PVDF membrane. Target proteins were sequentially immunoblotted with relevant primary antibodies and fluorescent secondary antibodies (LI-COR Biosciences), followed by measuring fluorescent intensity with a LI-COR Odyssey blot imager (LI-COR Biosciences). The eventual samples for Western blotting were pooled from three different experiments. Quantification of ubiquitination signals of blots showing in Fig. 2 (E and F) was performed to the area above 50 kDa.

Reverse-transcription quantitative PCR
Total RNA was extracted using the RNeasy mini kit (QIAGEN) as directed. A Tetro complementary DNA synthesis kit (Bioline) was used for reverse transcription. Subsequent qPCR was performed using PowerUp SYBR Green Master Mix (Applied Biosystems) in the QuantStudio 3 Real-Time PCR System (Thermo Fisher Scientific). The primers used for qPCR are listed in table S1. The amplification efficiency of all primers was tested and optimized. Gene expression was calculated with the delta-delta Ct ($\Delta\Delta Ct$) method normalized to the control gene encoding β-actin and glyceraldehyde-3-phosphate dehydrogenase, and all measurements were performed in triplicate.

Luciferase assay
Human embryonic kidney 293T cells were cultured in Dulbecco's modified Eagle's medium supplemented with 10% FBS, 2 mM glutamine,

penicillin (100 U/ml), and streptomycin (100 mg/ml). A total of 8×10^5 cells were seeded to each well of a six-well plate and transfected with the reporter vectors (400 ng), pSV40-*Renilla* luciferase vector (200 ng), and expression vectors (2 μg) using BioT transfection reagent (Bioland Scientific, Paramount, CA). The same amount of plasmid DNA was used by adjusting with an empty vector. Luciferase activity was measured using the Dual-Luciferase Reporter Assay System (Promega, Madison, WI) per the manufacturer's instruction and normalized against *Renilla* luciferase activities. "Relative luciferase activities" were plotted with further normalization of luciferase activities of each group to the pGL3-basic reporter vector plus the empty vector group. The generation of reporter plasmids was done by PCR amplification of *Runx1* genomic DNA containing the RORγt-binding region and a subsequent insertion upstream of a mini TK promoter that was cloned to pGL3-basic vector (Promega) for a minimal expression of luciferase. Cloning primers and mini TK promoter sequence are listed in table S1.

Statistical analysis

The ratio of rescue for thymocyte development and T_H17 differentiation in Fig. 2 (A and B) was calculated as relative ratio of the extent of *RORγt*$^{-/-}$ cells transduced with RORγt mutants to that of cells transduced with WT RORγt. The statistical parameters are indicated in the figure legends. The results were analyzed for statistical significance with unpaired Student's *t* test. Bodyweights are presented as means ± SD, and other data are shown as means ± SEM. *P* values are calculated using GraphPad Prism and presented where the statistical significance ($P < 0.05$) was found.

SUPPLEMENTARY MATERIALS

REFERENCES AND NOTES

1. Y. Lee, A. Awasthi, N. Yosef, F. J. Quintana, S. Xiao, A. Peters, C. Wu, M. Kleinewietfeld, S. Kunder, D. A. Hafler, R. A. Sobel, A. Regev, V. K. Kuchroo, Induction and molecular signature of pathogenic T_H17 cells. *Nat. Immunol.* **13**, 991–999 (2012).
2. L. Codarri, G. Gyulveszi, V. Tosevski, L. Hesske, A. Fontana, L. Magnenat, T. Suter, B. Becher, RORγt drives production of the cytokine GM-CSF in helper T cells, which is essential for the effector phase of autoimmune neuroinflammation. *Nat. Immunol.* **12**, 560–567 (2011).
3. M. El-Behi, B. Ciric, H. Dai, Y. Yan, M. Cullimore, F. Safavi, G. X. Zhang, B. N. Dittel, A. Rostami, The encephalitogenicity of T_H17 cells is dependent on IL-1- and IL-23-induced production of the cytokine GM-CSF. *Nat. Immunol.* **12**, 568–575 (2011).
4. M. M. Elloso, M. Gomez-Angelats, A. M. Fourie, Targeting the Th17 pathway in psoriasis. *J. Leukoc. Biol.* **92**, 1187–1197 (2012).
5. J. Skepner, R. Ramesh, M. Trocha, D. Schmidt, E. Baloglu, M. Lobera, T. Carlson, J. Hill, L. A. Orband-Miller, A. Barnes, M. Boudjelal, M. Sundrud, S. Ghosh, J. Yang, Pharmacologic inhibition of RORγt regulates Th17 signature gene expression and suppresses cutaneous inflammation in vivo. *J. Immunol.* **192**, 2564–2575 (2014).
6. G. B. Choi, Y. S. Yim, H. Wong, S. Kim, H. Kim, S. V. Kim, C. A. Hoeffer, D. R. Littman, J. R. Huh, The maternal interleukin-17a pathway in mice promotes autism-like phenotypes in offspring. *Science* **351**, 933–939 (2016).
7. I. I. Ivanov, B. S. McKenzie, L. Zhou, C. E. Tadokoro, A. Lepelley, J. J. Lafaille, D. J. Cua, D. R. Littman, The orphan nuclear receptor RORγt directs the differentiation program of proinflammatory IL-17$^+$ T helper cells. *Cell* **126**, 1121–1133 (2006).
8. Z. He, J. Ma, R. Wang, J. Zhang, Z. Huang, F. Wang, S. Sen, E. V. Rothenberg, Z. Sun, A two-amino-acid substitution in the transcription factor RORγt disrupts its function in T_H17 differentiation but not in thymocyte development. *Nat. Immunol.* **18**, 1128–1138 (2017).
9. Z. He, J. Zhang, Z. Huang, Q. Du, N. Li, Q. Zhang, Y. Chen, Z. Sun, Sumoylation of RORγt regulates T_H17 differentiation and thymocyte development. *Nat. Commun.* **9**, 4870 (2018).
10. S. Okada, J. G. Markle, E. K. Deenick, F. Mele, D. Averbuch, M. Lagos, M. Alzahrani, S. Al-Muhsen, R. Halwani, C. S. Ma, N. Wong, C. Soudais, L. A. Henderson, H. Marzouqa, J. Shamma, M. Gonzalez, R. Martinez-Barricarte, C. Okada, D. T. Avery, D. Latorre, C. Deswarte, F. Jabot-Hanin, E. Torrado, J. Fountain, A. Belkadi, Y. Itan, B. Boisson, M. Migaud, C. S. Arlehamn, A. Sette, S. Breton, J. McCluskey, J. Rossjohn, J. P. de Villartay, D. Moshous, S. Hambleton, S. Latour, P. D. Arkwright, C. Picard, O. Lantz, D. Engelhard, M. Kobayashi, L. Abel, A. M. Cooper, L. D. Notarangelo, S. Boisson-Dupuis, A. Puel, F. Sallusto, J. Bustamante, S. G. Tangye, J. L. Casanova, Impairment of immunity to *Candida* and *Mycobacterium* in humans with bi-allelic *RORC* mutations. *Science* **349**, 606–613 (2015).
11. S. Xiao, N. Yosef, J. Yang, Y. Wang, L. Zhou, C. Zhu, C. Wu, E. Baloglu, D. Schmidt, R. Ramesh, M. Lobera, M. S. Sundrud, P. Y. Tsai, Z. Xiang, J. Wang, Y. Xu, X. Lin, K. Kretschmer, P. B. Rahl, R. A. Young, Z. Zhong, D. A. Hafler, A. Regev, S. Ghosh, A. Marson, V. K. Kuchroo, Small-molecule RORγt antagonists inhibit T helper 17 cell transcriptional network by divergent mechanisms. *Immunity* **40**, 477–489 (2014).
12. Z. Huang, H. Xie, R. Wang, Z. Sun, Retinoid-related orphan receptor γt is a potential therapeutic target for controlling inflammatory autoimmunity. *Expert Opin. Ther. Targets* **11**, 737–743 (2007).
13. J. R. Huh, D. R. Littman, Small molecule inhibitors of RORγt: Targeting Th17 cells and other applications. *Eur. J. Immunol.* **42**, 2232–2237 (2012).
14. S. L. Gaffen, R. Jain, A. V. Garg, D. J. Cua, The IL-23-IL-17 immune axis: From mechanisms to therapeutic testing. *Nat. Rev. Immunol.* **14**, 585–600 (2014).
15. J. S. Bezbradica, T. Hill, A. K. Stanic, L. Van Kaer, S. Joyce, Commitment toward the natural T (iNKT) cell lineage occurs at the CD4$^+$8$^+$ stage of thymic ontogeny. *Proc. Natl. Acad. Sci. U.S.A.* **102**, 5114–5119 (2005).
16. A. V. Rachitskaya, A. M. Hansen, R. Horai, Z. Li, R. Villasmil, D. Luger, R. B. Nussenblatt, R. R. Caspi, Cutting edge: NKT cells constitutively express IL-23 receptor and RORγt and rapidly produce IL-17 upon receptor ligation in an IL-6-independent fashion. *J. Immunol.* **180**, 5167–5171 (2008).
17. T. Egawa, G. Eberl, I. Taniuchi, K. Benlagha, F. Geissmann, L. Hennighausen, A. Bendelac, D. R. Littman, Genetic evidence supporting selection of the Valpha14i NKT cell lineage from double-positive thymocyte precursors. *Immunity* **22**, 705–716 (2005).
18. Z. Sun, D. Unutmaz, Y. R. Zou, M. J. Sunshine, A. Pierani, S. Brenner-Morton, R. E. Mebius, D. R. Littman, Requirement for RORγ in thymocyte survival and lymphoid organ development. *Science* **288**, 2369–2373 (2000).
19. R. Wang, H. Xie, Z. Huang, J. Ma, X. Fang, Y. Ding, Z. Sun, Transcription factor network regulating CD$^+$CD8$^+$ thymocyte survival. *Crit. Rev. Immunol.* **31**, 447–458 (2011).
20. H. Xie, M. S. Sadim, Z. Sun, RORγt recruits steroid receptor coactivators to ensure thymocyte survival. *J. Immunol.* **175**, 3800–3809 (2005).
21. D. Komander, M. Rape, The ubiquitin code. *Annu. Rev. Biochem.* **81**, 203–229 (2012).
22. S. Rutz, N. Kayagaki, Q. T. Phung, C. Eidenschenk, R. Noubade, X. Wang, J. Lesch, R. Lu, K. Newton, O. W. Huang, A. G. Cochran, M. Vasser, B. P. Fauber, J. DeVoss, J. Webster, L. Diehl, Z. Modrusan, D. S. Kirkpatrick, J. R. Lill, W. Ouyang, V. M. Dixit, Deubiquitinase DUBA is a post-translational brake on interleukin-17 production in T cells. *Nature* **518**, 417–421 (2015).
23. L. Han, J. Yang, X. Wang, Q. Wu, S. Yin, Z. Li, J. Zhang, Y. Xing, Z. Chen, A. Tsun, D. Li, M. Piccioni, Y. Zhang, Q. Guo, L. Jiang, L. Bao, L. Lv, B. Li, The E3 deubiquitinase USP17 is a positive regulator of retinoic acid-related orphan nuclear receptor γt (RORγt) in Th17 cells. *J. Biol. Chem.* **289**, 25546–25555 (2014).
24. X. Wang, J. Yang, L. Han, K. Zhao, Q. Wu, L. Bao, Z. Li, L. Lv, B. Li, TRAF5-mediated Lys-63-linked polyubiquitination plays an essential role in positive regulation of RORγt in promoting IL-17A expression. *J. Biol. Chem.* **290**, 29086–29094 (2015).
25. J. Yang, P. Xu, L. Han, Z. Guo, X. Wang, Z. Chen, J. Nie, S. Yin, M. Piccioni, A. Tsun, L. Lv, S. Ge, B. Li, Cutting edge: Ubiquitin-specific protease 4 promotes Th17 cell function under inflammation by deubiquitinating and stabilizing RORγt. *J. Immunol.* **194**, 4094–4097 (2015).
26. H. Hu, S. C. Sun, Ubiquitin signaling in immune responses. *Cell Res.* **26**, 457–483 (2016).
27. R. Holmes, J. C. Zúñiga-Pflücker, The OP9-DL1 system: Generation of T-lymphocytes from embryonic or hematopoietic stem cells in vitro. *Cold Spring Harb. Protoc.* **2009**, pdb. prot5156 (2009).
28. E. Bettelli, M. Pagany, H. L. Weiner, C. Linington, R. A. Sobel, V. K. Kuchroo, Myelin oligodendrocyte glycoprotein-specific T cell receptor transgenic mice develop spontaneous autoimmune optic neuritis. *J. Exp. Med.* **197**, 1073–1081 (2003).
29. L. Wu, K. E. R. Hollinshead, Y. Hao, C. Au, L. Kroehling, C. Ng, W. Y. Lin, D. Li, H. M. Silva, J. Shin, J. J. Lafaille, R. Possemato, M. E. Pacold, T. Papagiannakopoulos, A. C. Kimmelman, R. Satija, D. R. Littman, Niche-selective inhibition of pathogenic Th17 cells by targeting metabolic redundancy. *Cell* **182**, 641–654.e20 (2020).
30. I. M. Stromnes, J. M. Goverman, Active induction of experimental allergic encephalomyelitis. *Nat. Protoc.* **1**, 1810–1819 (2006).
31. Z. He, J. Zhang, Q. Du, J. Xu, Y. Gwack, Z. Sun, SRC3 is a cofactor for RORγt in Th17 differentiation but not thymocyte development. *J. Immunol.* **202**, 760–769 (2019).
32. R. Wang, H. Xie, Z. Huang, J. Ma, X. Fang, Y. Ding, Z. Sun, T cell factor 1 regulates thymocyte survival via a RORγt-dependent pathway. *J. Immunol.* **187**, 5964–5973 (2011).

33. D. J. Cua, J. Sherlock, Y. Chen, C. A. Murphy, B. Joyce, B. Seymour, L. Lucian, W. To, S. Kwan, T. Churakova, S. Zurawski, M. Wiekowski, S. A. Lira, D. Gorman, R. A. Kastelein, J. D. Sedgwick, Interleukin-23 rather than interleukin-12 is the critical cytokine for autoimmune inflammation of the brain. *Nature* **421**, 744–748 (2003).

34. K. Xu, N. Yin, M. Peng, E. G. Stamatiades, S. Chhangawala, A. Shyu, P. Li, X. Zhang, M. H. Do, K. J. Capistrano, C. Chou, C. S. Leslie, M. O. Li, Glycolytic ATP fuels phosphoinositide 3-kinase signaling to support effector T helper 17 cell responses. *Immunity* **54**, 976–987.e7 (2021).

35. J. T. Gaublomme, N. Yosef, Y. Lee, R. S. Gertner, L. V. Yang, C. Wu, P. P. Pandolfi, T. Mak, R. Satija, A. K. Shalek, V. K. Kuchroo, H. Park, A. Regev, Single-cell genomics unveils critical regulators of Th17 cell pathogenicity. *Cell* **163**, 1400–1412 (2015).

36. M. Ciofani, A. Madar, C. Galan, M. Sellars, K. Mace, F. Pauli, A. Agarwal, W. Huang, C. N. Parkurst, M. Muratet, K. M. Newberry, S. Meadows, A. Greenfield, Y. Yang, P. Jain, F. K. Kirigin, C. Birchmeier, E. F. Wagner, K. M. Murphy, R. M. Myers, R. Bonneau, D. R. Littman, A validated regulatory network for Th17 cell specification. *Cell* **151**, 289–303 (2012).

37. Y. Wang, J. Godec, K. Ben-Aissa, K. Cui, K. Zhao, A. B. Pucsek, Y. K. Lee, C. T. Weaver, R. Yagi, V. Lazarevic, The transcription factors T-bet and Runx are required for the ontogeny of pathogenic interferon-γ-producing T helper 17 cells. *Immunity* **40**, 355–366 (2014).

38. P. R. Mangan, L. E. Harrington, D. B. O'Quinn, W. S. Helms, D. C. Bullard, C. O. Elson, R. D. Hatton, S. M. Wahl, T. R. Schoeb, C. T. Weaver, Transforming growth factor-β induces development of the T_H17 lineage. *Nature* **441**, 231–234 (2006).

39. M. Veldhoen, R. J. Hocking, C. J. Atkins, R. M. Locksley, B. Stockinger, TGFβ in the context of an inflammatory cytokine milieu supports de novo differentiation of IL-17-producing T cells. *Immunity* **24**, 179–189 (2006).

40. P. Miossec, T. Korn, V. K. Kuchroo, Interleukin-17 and type 17 helper T cells. *N. Engl. J. Med.* **361**, 888–898 (2009).

41. T. Korn, E. Bettelli, M. Oukka, V. K. Kuchroo, IL-17 and Th17 Cells. *Annu. Rev. Immunol.* **27**, 485–517 (2009).

42. T. Okuda, M. Nishimura, M. Nakao, Y. Fujita, RUNX1/AML1: A central player in hematopoiesis. *Int. J. Hematol.* **74**, 252–257 (2001).

43. T. Egawa, R. E. Tillman, Y. Naoe, I. Taniuchi, D. R. Littman, The role of the Runx transcription factors in thymocyte differentiation and in homeostasis of naive T cells. *J. Exp. Med.* **204**, 1945–1957 (2007).

44. T. Okuda, J. van Deursen, S. W. Hiebert, G. Grosveld, J. R. Downing, AML1, the target of multiple chromosomal translocations in human leukemia, is essential for normal fetal liver hematopoiesis. *Cell* **84**, 321–330 (1996).

45. R. Sood, Y. Kamikubo, P. Liu, Role of RUNX in hematological malignancies. *Blood* **129**, 2070–2082 (2017).

46. V. Lazarevic, X. Chen, J. H. Shim, E. S. Hwang, E. Jang, A. N. Bolm, M. Oukka, V. K. Kuchroo, L. H. Glimcher, T-bet represses T_H17 differentiation by preventing Runx1-mediated activation of the gene encoding RORγt. *Nat. Immunol.* **12**, 96–104 (2011).

47. L. Li, N. Patsoukis, V. Petkova, V. A. Boussiotis, Runx1 and Runx3 are involved in the generation and function of highly suppressive IL-17-producing T regulatory cells. *PLOS ONE* **7**, e45115 (2012).

48. M. Martinez, M. Hinojosa, D. Trombly, V. Morin, J. Stein, G. Stein, A. Javed, S. E. Gutierrez, Transcriptional auto-regulation of RUNX1 P1 promoter. *PLOS ONE* **11**, e0149119 (2016).

49. K. Yasuda, Y. Takeuchi, K. Hirota, The pathogenicity of Th17 cells in autoimmune diseases. *Semin. Immunopathol.* **41**, 283–297 (2019).

50. K. Ghoreschi, A. Laurence, X. P. Yang, C. M. Tato, M. J. McGeachy, J. E. Konkel, H. L. Ramos, L. Wei, T. S. Davidson, N. Bouladoux, J. R. Grainger, Q. Chen, Y. Kanno, W. T. Watford, H. W. Sun, G. Eberl, E. M. Shevach, Y. Belkaid, D. J. Cua, W. Chen, J. J. O'Shea, Generation of pathogenic T_H17 cells in the absence of TGF-β signalling. *Nature* **467**, 967–971 (2010).

51. C. L. Langrish, Y. Chen, W. M. Blumenschein, J. Mattson, B. Basham, J. D. Sedgwick, T. McClanahan, R. A. Kastelein, D. J. Cua, IL-23 drives a pathogenic T cell population that induces autoimmune inflammation. *J. Exp. Med.* **201**, 233–240 (2005).

52. G. Tonel, C. Conrad, U. Laggner, P. Di Meglio, K. Grys, T. K. McClanahan, W. M. Blumenschein, J. Z. Qin, H. Xin, E. Oldham, R. Kastelein, B. J. Nickoloff, F. O. Nestle, Cutting edge: A critical functional role for IL-23 in psoriasis. *J. Immunol.* **185**, 5688–5691 (2010).

53. C. Fotiadou, E. Lazaridou, E. Sotiriou, D. Ioannides, Targeting IL-23 in psoriasis: Current perspectives. *Psoriasis (Auckl)* **8**, 1–5 (2018).

54. J. Hanzel, G. R. D'Haens, Anti-interleukin-23 agents for the treatment of ulcerative colitis. *Expert Opin. Biol. Ther.* **20**, 399–406 (2020).

55. A. R. Moschen, H. Tilg, T. Raine, IL-12, IL-23, and IL-17 in IBD: Immunobiology and therapeutic targeting. *Nat. Rev. Gastroenterol. Hepatol.* **16**, 185–196 (2019).

56. B. M. Segal, C. S. Constantinescu, A. Raychaudhuri, L. Kim, R. Fidelus-Gort, L. H. Kasper; Ustekinumab MS Investigators, Repeated subcutaneous injections of IL12/23 p40 neutralising antibody, ustekinumab, in patients with relapsing-remitting multiple sclerosis: A phase II, double-blind, placebo-controlled, randomised, dose-ranging study. *Lancet Neurol.* **7**, 796–804 (2008).

57. C. Sheridan, Footrace to clinic heats up for T-cell nuclear receptor inhibitors. *Nat. Biotechnol.* **31**, 370 (2013).

58. E. Ueda, S. Kurebayashi, M. Sakaue, M. Backlund, B. Koller, A. M. Jetten, High incidence of T-cell lymphomas in mice deficient in the retinoid-related orphan receptor RORγ. *Cancer Res.* **62**, 901–909 (2002).

59. M. Liljevald, M. Rehnberg, M. Soderberg, M. Ramnegard, J. Borjesson, D. Luciani, N. Krutrok, L. Branden, C. Johansson, X. Xu, M. Bjursell, A. K. Sjogren, J. Hornberg, U. Andersson, D. Keeling, J. Jirholt, Retinoid-related orphan receptor γ (RORγ) adult induced knockout mice develop lymphoblastic lymphoma. *Autoimmun. Rev.* **15**, 1062–1070 (2016).